LASER RAMAN PROBE FOR FLAME TEMPERATURE

Marshall Lapp, et al

Purdue University

Prepared for:

Office of Naval Research

April 1973

PROJECT SQUID

TECHNICAL REPORT GE-1-PU

LASER RAMAN PROBE FOR FLAME TEMPERATURE

BY

MARSHALL LAPP
CARL M. PENNEY and RICHARD L. ST. PETERS
GENERAL ELECTRIC CO.
CORPORATE RESEARCH AND DEVELOPMENT
SCHENECTADY NEW YORK

PROJECT SQUID HEADQUARTERS
THERMAL SCIENCE AND PROPULSION CENTER
PURDUE UNIVERSITY
WEST LAFAYETTE, INDIANA

APRIL 1973

Project SQUID is a cooperative program of basic research relating to Jet Propulsion. It is sponsored by the Office of Naval Research and is administered by Purdue University through Contract N00014-67-A-0226-0005, NR-098-038.

Unclassified

Security Classification

DOCUMENT CONTROL DATA - R & D

(Security classification of title, body of abstract and indexing annotation must be entered when the overall report is classified)

1. ORIGINATING ACTIVITY (Corporate author)
Project SQUID Headquarters, Thermal Science & Propulsion Center, Purdue University, West Lafayette, Indiana 47907

2a. REPORT SECURITY CLASSIFICATION
Unclassified

2b. GROUP
N/A

3. REPORT TITLE

LASER RAMAN PROBE FOR FLAME TEMPERATURE

4. DESCRIPTIVE NOTES (Type of report and inclusive dates)

5. AUTHOR(S) (First name, middle initial, last name)
Marshall Lapp
Carl M. Penney
Richard L. St.Peters

6. REPORT DATE
April 1973

7a. TOTAL NO. OF PAGES
52 54

7b. NO. OF REFS
4

8a. CONTRACT OR GRANT NO.
N00014-67-A-0226-0005

b. PROJECT NO.
NR-098-038

c.

d.

9a. ORIGINATOR'S REPORT NUMBER(S)
GE-1-PU

9b. OTHER REPORT NO(S) (Any other numbers that may be assigned this report)
None

10. DISTRIBUTION STATEMENT

This document has been approved for public release and sale; its distribution is unlimited.

11. SUPPLEMENTARY NOTES
N/A

Details of illustrations in this document may be better studied on microfiche.

12. SPONSORING MILITARY ACTIVITY
Office of Naval Research, Power Program, Code 473, Department of the Navy, Arlington, Virginia 22217

13. ABSTRACT

Experimental spectra of Raman Scattering Stokes fundamental vibrational Q-branches for nitrogen and hydrogen in hydrogen-air flames have been fit to theoretically-calculated profiles in order to determine temperature. The temperature measured from a least square fit of the full nitrogen profile agreed to within about ½% of the value calculated from the ratio of the peak intensity of the first upper state band (i.e., "hot" band) to that of the ground state band. Agreement with the temperature estimated from fine-wire thermocouple measurements was approximately 2%. Additional theoretical profile calculations are given from nitrogen and hydrogen over the wide range of temperatures.

DD FORM 1 NOV 65 1473 (PAGE 1)

S/N 0101-807-6801

Unclassified

Security Classification

14. KEY WORDS	LINK A		LINK B		LINK C	
	ROLE	WT	ROLE	WT	ROLE	WT
Raman Scattering						
Combustion						
Flame						
Spectroscopy						
Sensors						
Lasers						

LASER RAMAN PROBE FOR FLAME TEMPERATURE

General Electric Co., Corporate Research and Development
Schenectady, New York
Subcontract No. 4965-38

Marshall Lapp, Principal Investigator

Carl M. Penney, Physicist
Richard L. St.Peters, Physicist

Introduction

This work is directed toward the measurement of vibrational Raman scattering signatures for flame gases, with a primary view toward temperature measurements and a concommitant goal of identification and measurement of minor flame species. The development of an optical probe for those purposes is highly desirable, since advanced combustion systems are utilizing pressures and temperatures such that physical probes cannot survive. The use of a Raman scattering probe, in particular, offers a variety of advantages over other optical probes, along with some limitations which will be explored during the course of this work.

During this project reporting period, experimental effort has been focussed mainly on: (1) the observation and fitting of Raman Stokes vibrational Q-branch profiles for N_2 and H_2 obtained through

use of H_2-air flames produced on porous plug burners, (2) exploration of the accuracy of temperature measurement for N_2 through extended thermocouple calibrations and computer data-fitting techniques, and (3) construction and preliminary use of apparatus designed for use in these and other phases of this research project.

The theoretical effort during this project reporting period has been concentrated upon analytical calculations of Raman Stokes vibrational Q-branch profiles, suitably convoluted by experimentally-determined monochromator slit functions or interference filter bandpasses. The main effort has involved analytical procedures necessary to determine the temperature, and has included both least-square data fitting of entire profiles as well as intensity ratios of suitably chosen spectral regions.

I. Experimental Equipment

The basic double monochromator experimental apparatus has been described previously.[1] (Ref. 1 is included here as Appendix 1.) New additions have been made to the combustion, spectroscopic, temperature-measurement and computer data handling capabilities in connection with several parallel programs in our laboratory. Those which pertain directly to the present research effort are described next in outline fashion:

(1) A horizontal hydrogen-oxygen burner system utilizing a Meker burner has been assembled, which will permit flames to be produced up to ca. 3000°K. This apparatus does not disturb the basic geometry of our double-monochromator system, since it permits use of a vertical laser beam passing through the flame in the same fashion as for our porous plug burner assembly used at ca. 1300-1700°K. The high-temperature burner is designed for production of "minor" flame species of high technological interest, such as OH. Preliminary design studies have also been carried out for auxiliary optics for utilization with a vertically burning flame. In this configuration, a line image (i.e., the scattering zone in the flame) must be rotated through 90 degrees. Design studies include both use of two additional mirrors and use of a Dove prism.

(2) Accurate flow metering techniques have been installed for the production of reproducible and clearly-defined flame conditions. The flows are now monitored and made steady by critical flow orifices and regulators, use being made of precision high-pressure gauges for accurate control of the flow rates. The critical flow orifices have been calibrated in our laboratory through use of basic volume-displacement techniques.

(3) Fine wire thermocouples have been made in our laboratory for independent measurements of the flame temperature by a standard method. These thermocouples[2] were made of 0.0005 inch diameter wires of Pt - Pt 10% Rh, coated with quartz to prevent catalytic heating. The thermocouples were moved throughout the flame with an accurate vernier manipulator using, as a reference position locator, a finely-machined metal cone which could be placed reproducibly on the burner head. When the burner assembly was then placed in the test position in front of the spectrometer, the burner could be accurately located in this same reference position by placing it so that the laser beam just touched the cone tip. (By observing slight attenuation of the laser beam with a power meter at the position of the laser dump, this positioning could be accomplished with high sensitivity.)

In principle, the thermocouple-measurement position and laser Raman scattering position could be made coincident by imaging the laser beam on the thermocouple junction. However, it is experimentally difficult to accomplish this. In addition, the thermocouples are relatively fragile, and it was therefore found to be advisable to calibrate the flame before embarking on the scattering measurements.

Additional temperature measurements have been made with a commercially-available 0.001 inch diameter Pt - Pt 10% Rh thermocouple with a bead-welded end, stretched out to the same linear geometry as was used for the 0.0005 inch diameter thermocouples described above. (See Fig. 1 for schematics of these two types of thermocouples.) This thermocouple was not quartz-clad, but had longer leads. The basic idea was to test the sensitivity of thermocouple measurement of temperature to thermocouple geometry, without embarking upon a major

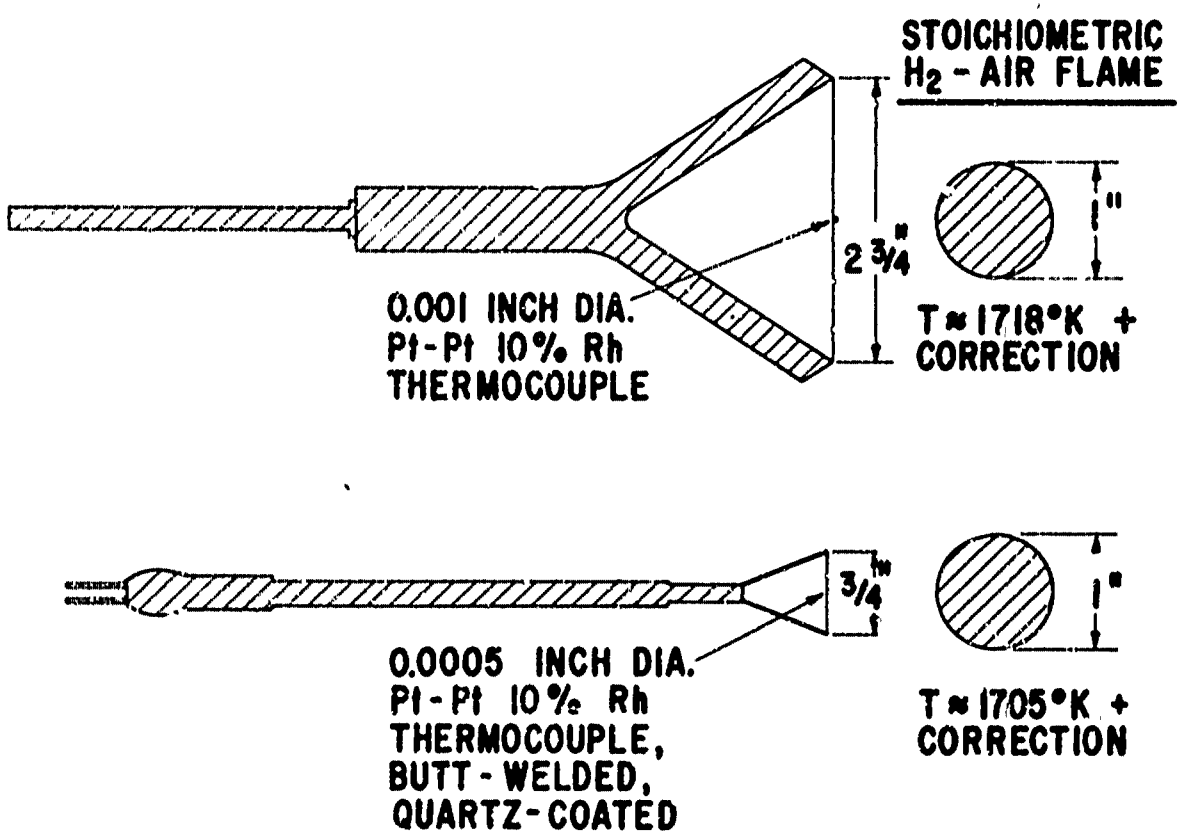

Fig. 1 Schematics of thermocouples used for flame temperature calibrations. (The flame temperatures quoted are from a study in which thermocouples were compared, and do not correspond to the exact conditions for which the Raman scattering data and subsequent thermocouple temperature measurements were made.)

diversion of effort. The result was that a modest but not very significant difference existed. The smaller thermocouple gave an uncorrected temperature of 1705°K in a carefully controlled stoichiometric hydrogen-air flame, while the larger gave 1718°K. These values are the average of many measurements with only a small variation between measurements. Since the correction for radiative losses (the largest correction here) to be applied to thermocouple-measured temperatures is ca. 4 times larger than this difference of values, the difference is not believed to be highly significant.

(4) Data logging via paper tape for intensity and wavelength has been installed in the double monochromator system. This apparatus permits data to be accumulated in a far more accurate and convenient fashion, making full use of our computer facilities. In Fig. 2 is shown the electronic detection schematic for this apparatus. The wavelength data is obtained through use of an optical incremental encoder installed on the double monochromator. This system, now operational, is currently being improved by location of a new optical encoder element directly on the wavelength screw (rather than in a more remote mechanical location, as is presently the case). The encoding of accurate wavelength data is considered important because use of an inaccurate (non-linear, etc.) wavelength axis in fitting experimental Raman vibrational Q-branch profiles to theoretical shapes results in distortion which, in turn, lead to inaccurate computer fits and therefore inaccurate temperatures.

(5) An interference filter-test cell apparatus has been constructed which is capable of operation with a porous plug burner. A photograph of the apparatus appears as Fig. 3, while a schematic is shown in Fig. 4.

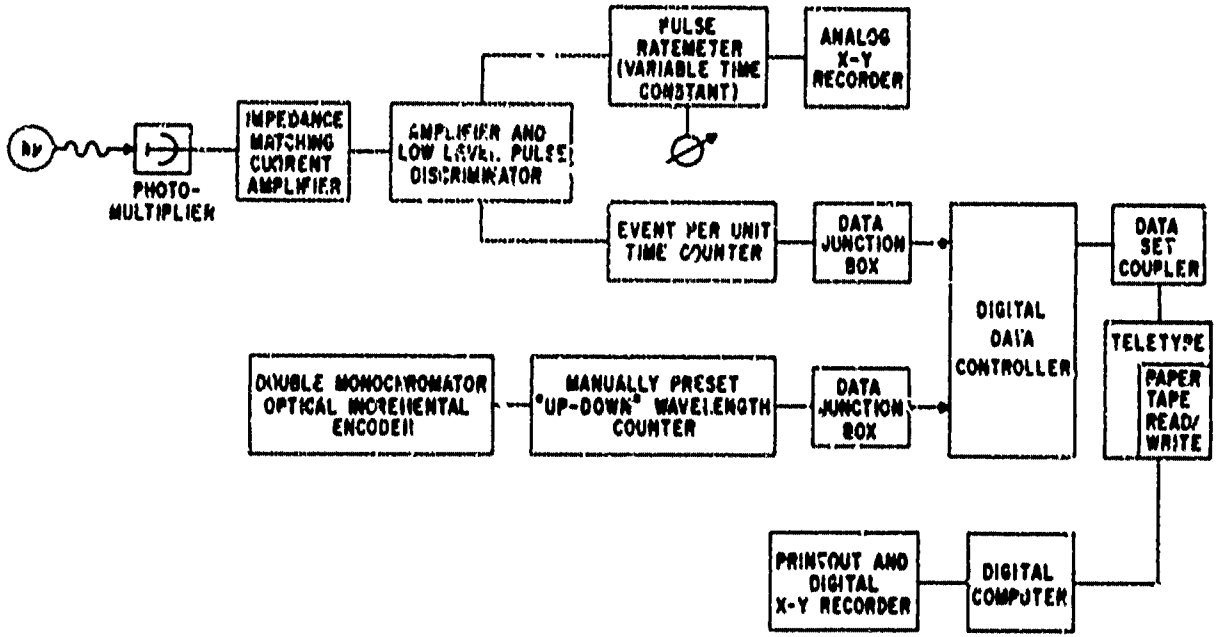

Fig. 2 Electronic detection apparatus for double monochromator, including photon counting equipment, digital intensity and wavelength data encoding equipment, and computer processing equipment. Photons (labeled "hν") are shown leaving the exit slits of the double monochromator.

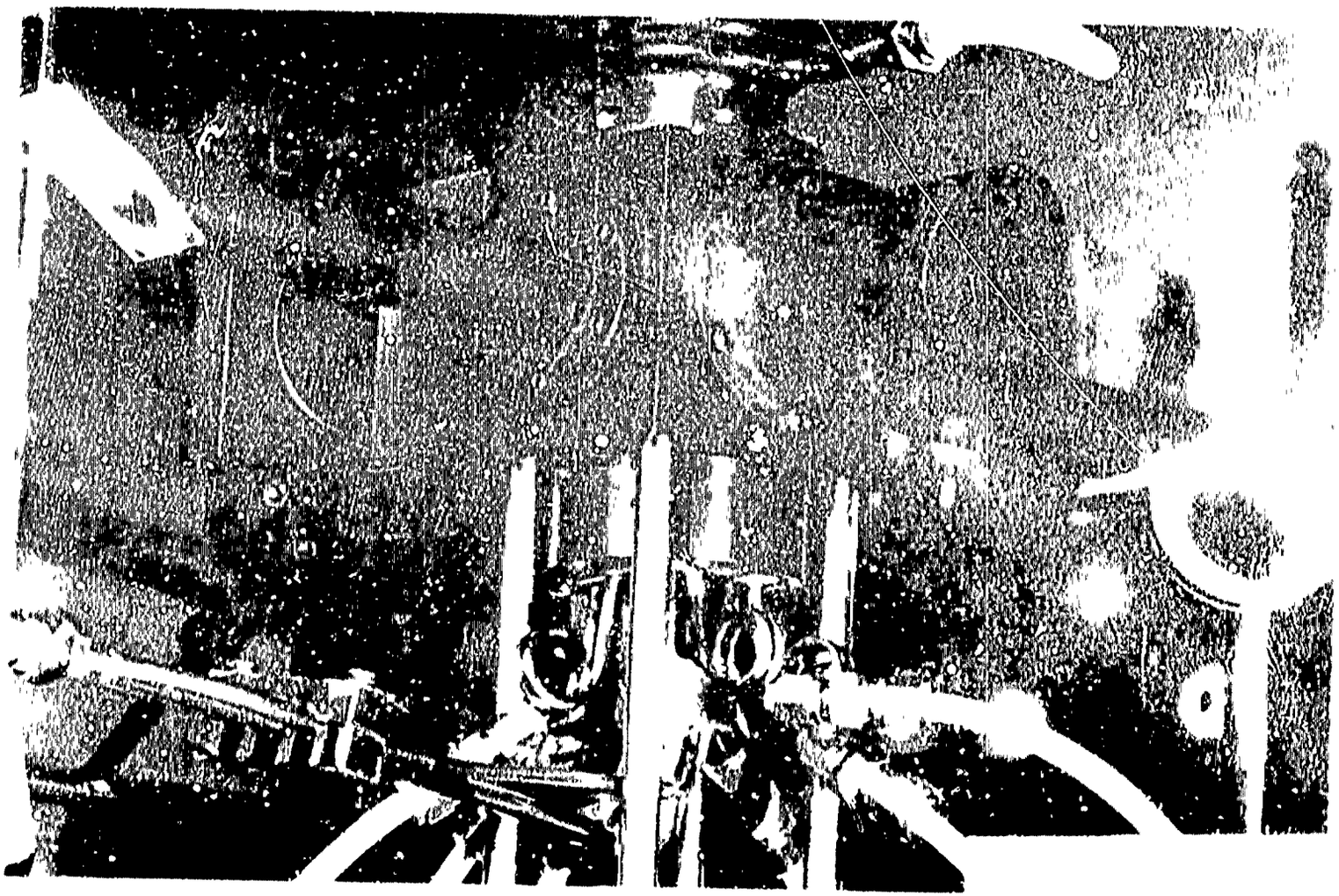

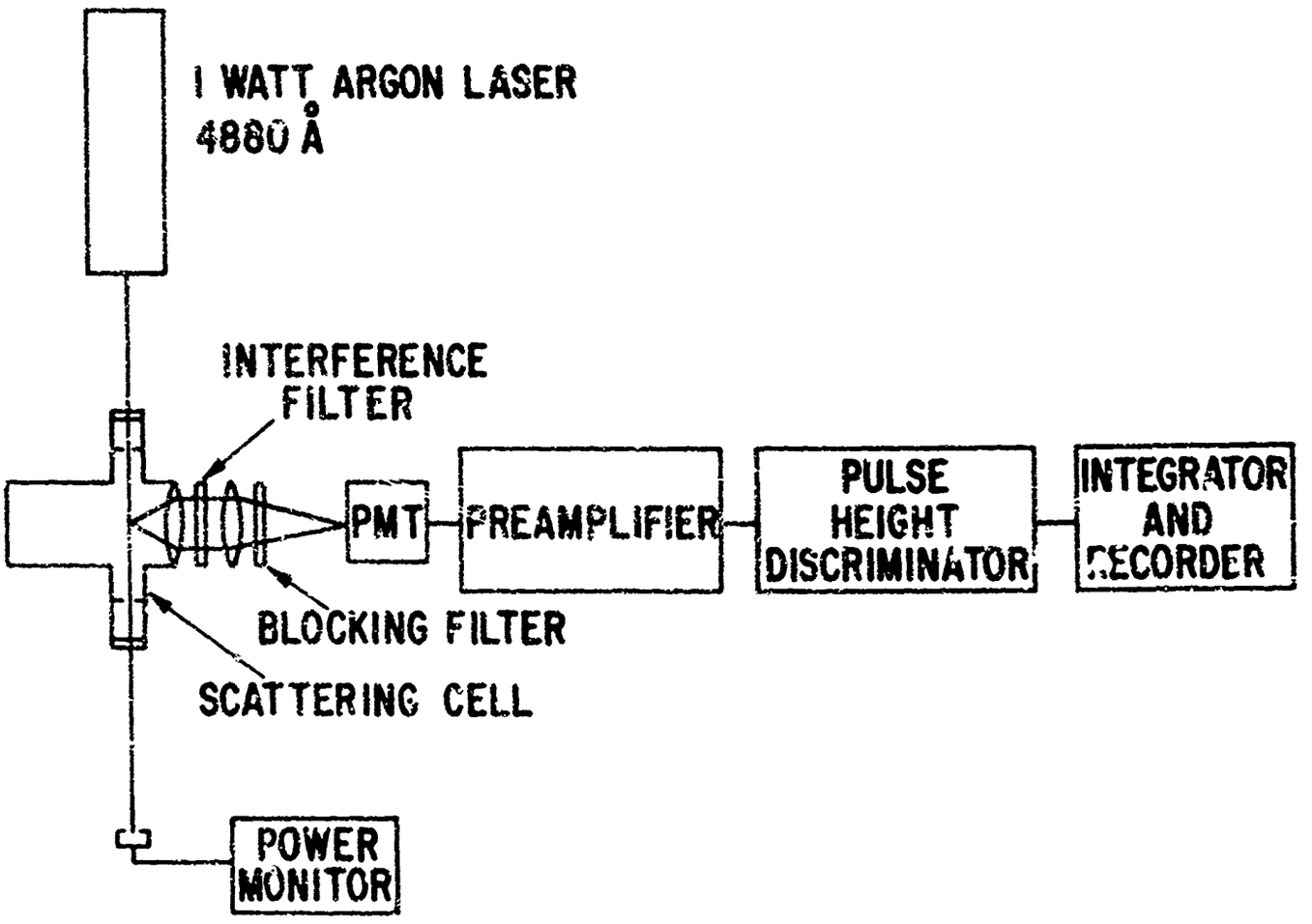

Fig. 4 Schematic of interference filter-test cell apparatus designed for photon-counting operation.

Preliminary operation of this test cell with several hydrogen-oxygen flames has identified areas of needed additional development work. Particular attention is now being given to cooling of the interference filters, since the filter passbands shift with the temperature, and do not return to their initial positions when the original temperature is restored.

II. Experimental Conditions

All experiments discussed here utilized the double monochromator and horizontally-burning hydrogen-air flames on a 2.5 cm-diameter water cooled porous plug burner which was placed 2.0 cm away from another water-cooled porous plug connected to a vacuum line. A continuous wave argon ion laser source of about 1 watt at the flame position at 488 nm was used for all the results reported here. The temperatures of the flames were measured as a function of position by means of the fine thermocouples described in the previous section.

Two different flames were studied. First, for nitrogen data, a steady stoichiometric hydrogen-air flame was utilized (37.5 cc/sec. H_2 and 88.8 cc/sec. air) for which 65% of the product gases was nitrogen. The flame was found to be about 1575°K at its center point (i.e., halfway between the burner head and the vacuum plug), including a rough 50°K correction for thermocouple radiative losses. Since the image of the monochromator entrance slits at the flame scattering position was about 5 mm high, an estimate was made of the temperature variation along this zone. This was found to be about 16°K. The reproducibility of the thermocouple data was about ± 4°K.

Second, for hydrogen data, a less steady fuel-rich (four times stoichiometric) hydrogen-air flame was used (79.3 cc/sec. H_2 and 47.0 cc/sec. air) for which about 51% of the product gases was hydrogen. This flame was found to be about 1390°K at its center point, including a rough 40°K correction for radiative losses. Here, the variation of temperature with position along the slit image was much more severe, being roughly 110°K over a 5 mm vertical zone. Furthermore, the reproducibility was significantly poorer, being roughly ± 3°K. This flame, colored red from the emission of water vapor vibration-rotation bands,[3] was subject to significantly more diffusion by the ambient atmosphere than the preceeding flame, which undoubtedly contributed to its less reproducible characteristics. It had, however, the virtue of a high hydrogen content.

III. Theoretical Predictions of Band Profiles

For the diatomic molecules considered in these experiments, Eq. (3) of Ref. 1 (see Appendix 1) can be used for the calculation of the Stokes Q-branch fundamental series ($v+1 \leftarrow v$) profiles. This intensity relation neglects the small depolarized contribution for our cases. The profiles calculated in Ref. 1 in this fashion were used to fit experimental profiles in order to determine the scattering-gas temperature. Therefore, all calculated profiles were normalized to the experimental curve peaks. Such normalized profiles are also used here in computer fits for temperature determination (see Fig. 13), but for other purposes, it is desired to calculate profiles for a given molecule at various temperatures while maintaining the spectral intensity differences at these temperatures

(i.e., not normalizing each profile at the peak intensity). This is the case, for example, if it is desired to calculate the relative intensities at different temperatures obtained through use of a monochromator or filter designed to isolate a spectral portion of the Q-branch. We point out here that Eq. (3) of Ref. 1 can be used for these calculations if the vibrational partition function Q_{vib} given in Ref. 1 following Eq. (3),

$$Q_{vib} \approx [1-\exp(-hc\omega_e/kT)]^{-1},$$

is multiplied by the factor $\exp[-(hc/kT)G(0,0)]$, where $G(0,0)$ is the zero-point energy. Here:

$$G(0,0) = (1/2)\omega_e - (1/4)\omega_e x_e + (1/8)\omega_e y_e$$

where ω_e, $\omega_e x_e$, and $\omega_e y_e$ are vibrational constants defined by Eq. (1) of Ref. 1. The exponential factor compensates for the fact that the term value $G(v,J)$ defined by Eq. (1) of Ref. 1 relates to the energy above zero rather than above the zero-point energy.

Furthermore, substitution of ω_o for ω_e in Eq. (1) for Q_{vib}, where

$$\omega_o \approx \omega_e - \omega_e x_e + (3/4)\,\omega_e y_e$$

results in a slightly more accurate calculation of Q_{vib}. Here, ω_o is the coefficient of the linear v term in the term value expression

$$G_o(v) = \omega_o v - \text{constant } x(v^2) + \ldots$$

Finally, if comparisons of Q-branch intensities are to be made between different molecules, account must be taken of the absolute

value of the nuclear spin statistical weight g_I. This may be accomplished by substitution of g_I for the relative factor n in Eq. (3) of Ref. 1, and, for $^1\Sigma$ states of homonuclear molecules, multiplication of the value of $Q_{rot} \approx kT, 2hcB_e$ given in Ref. 1 following Eq. (3), by the factor $(2I+1)^2$. Here, I is the nuclear spin quantum number.

In analogy with the previous comment on Q_{vib}, substitution of B_o for B_e in the relation for Q_{rot} results in a slightly more accurate calculation of Q_{rot}. Here,

$$B_o \approx B_e - \alpha_e/2$$

where α_e is the coefficient of the vibration-rotation interaction term in the term value G(v,J) given in Eq. (1) of Ref. 1.

In Fig. 5(A) are shown the calculated nitrogen rotational lines of the vibrational Q-branch at 1000°K, different symbols denoting the various fundamental bands. The nitrogen spectrum has alternately "strong" and "weak" lines because of nuclear spin degeneracy, but only the "strong" lines are shown here for clarity. In Fig. 5(B) is shown the spectrometer slit-convoluted intensity appropriate for the instrument used in our work, viz., a triangular slit function of full width at half maximum (FWHM) $\Delta = 1.63\text{Å}$ corresponding to 300μm entrance and exit slits on a Spex 1400-II double spectrometer. The same type of calculations for 2000°K and 3000°K are shown in Figs. 6 and 7, respectively.

Use of the type of data shown in Figs. 5-7 permits estimation of appropriate spectral regions for measuring the various rotational and vibrational excitation temperatures possible. In general, vibrational temperatures are proportional to the integral of intensity for particular bands (i.e., the ground state band or any specific upper state

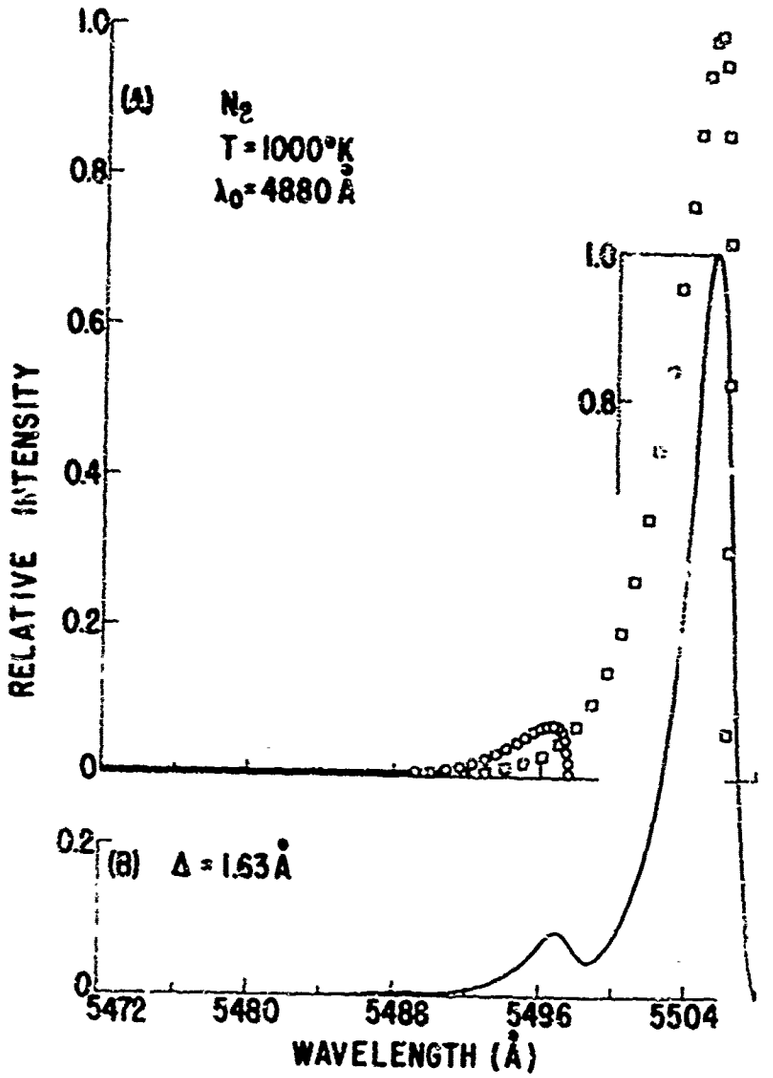

Fig. 5 Calculated Stokes Q-branch fundamental intensity at 1000°K for nitrogen. (A) Alternate "strong" line intensities. The square data points correspond to the ground state band and the circular points to the first upper state band. (B) Triangular slit function-convoluted profile, where Δ is the spectral slit width (FWHM).

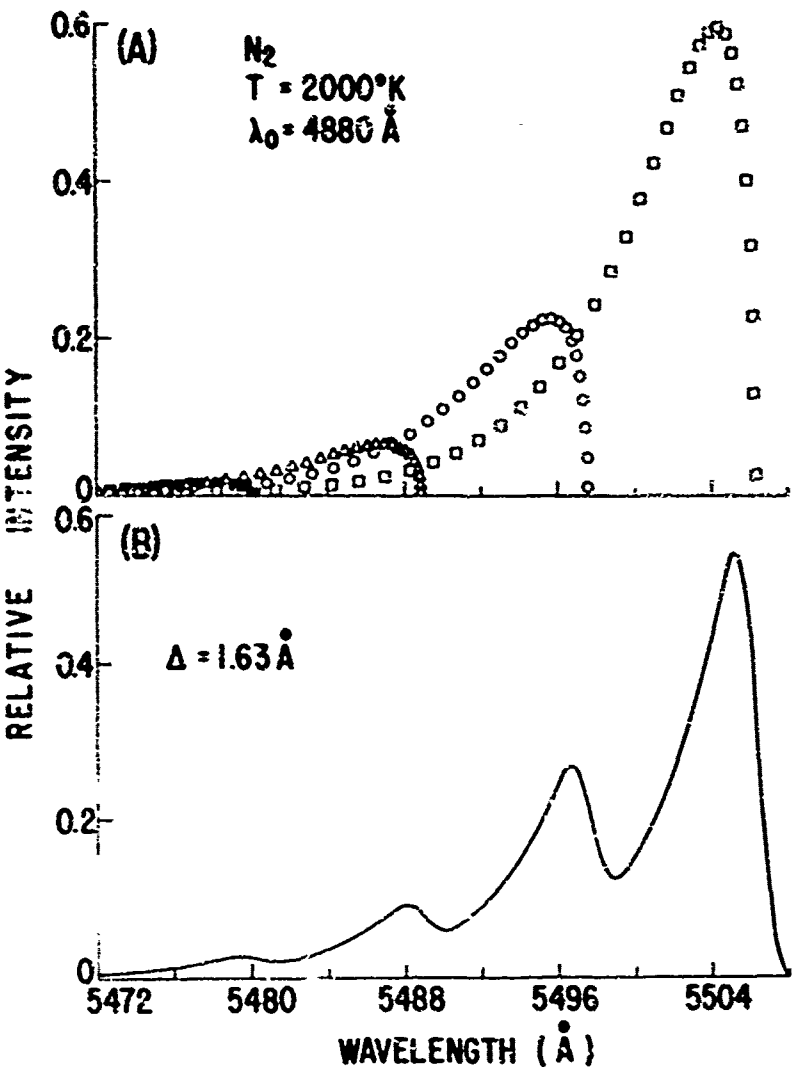

Fig. 6 Calculated Stokes Q-branch fundamental intensity at 2000°K for nitrogen. (A) Alternate "strong" line intensities. The square data points correspond to the ground state band, the circular points to the first upper state band, the open triangular points to the second upper state band, etc. (B) Triangular slit function convoluted profile, where Δ is the spectral slit width (FWHM).

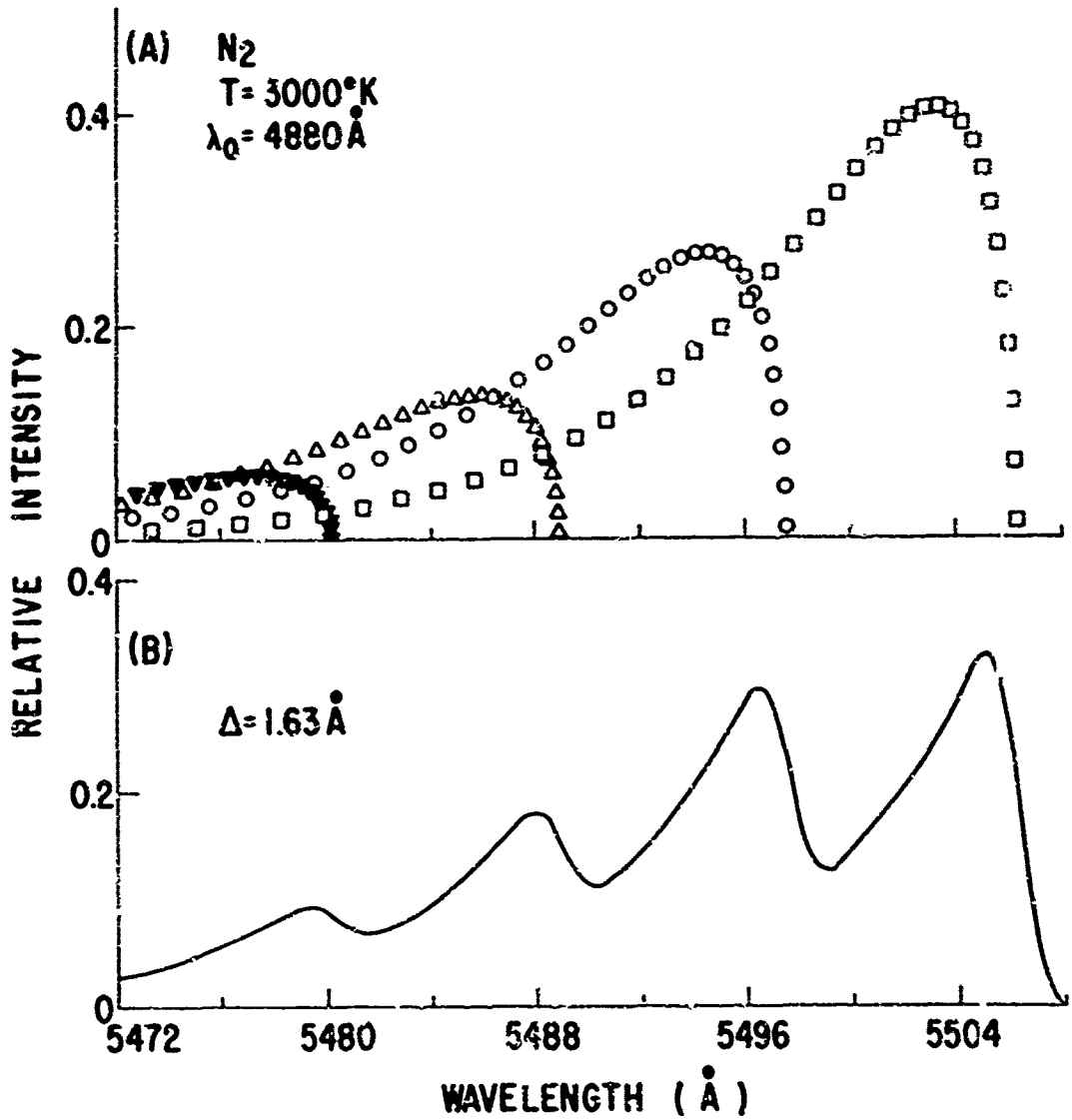

Fig. 7 Calculated Stokes Q-branch fundamental intensity at 3000°K for nitrogen. (A) Alternate "strong" line intensities. The square data points correspond to the ground state band, the circular points to the first upper state band, the open triangular points to the second upper state band, etc. (B) Triangular slit function convoluted profile, where Δ is the spectral slit width (FWHM)

band), while rotational temperatures are proportional to the profile on the short wavelength side of each band via the influence of the vibration-rotation interaction. Thus, in principle, it is possible to determine vibrational excitation temperatures for any pair of vibrational levels, and rotational excitation temperatures associated with any vibrational level.

For general comparative purposes, the nitrogen profile has been calculated from 300°K to 3500°K in Fig. 8 for $\Delta = 1.5\text{Å}$. Here, the relatively broad spectral width at elevated temperatures becomes quite apparent.

The profiles for hydrogen are very different from those for nitrogen, since the individual vibration-rotation lines of the Q-branch for light molecules are spread far apart because of their very large vibration-rotation interaction constant, α_e. (For hydrogen, α_e is over 10^2 times larger than the value for nitrogen.) In Fig. 9 are shown calculated shapes for hydrogen from 300°K to 1500°K, while in Fig. 10 are shown the profiles for 1900°K to 3500°K. We note that the first vibration-rotation line of the first upper state band in hydrogen does not appear for a <u>longer</u> spectral interval [starting from the (0,0) position, where the parenthetic notation corresponds to the lower level quantum numbers (v,J)] than that corresponding to the <u>entire</u> wavelength scale of all the nitrogen data plotted in Fig. 8.

IV. Experimental Results for Nitrogen

The profile of nitrogen observed from the stoichiometric flame at a thermocouple-measured temperature of 1575°K (1525°K indicated temperature, plus an estimated 50°K correction for radiative losses) is shown in Fig. 11

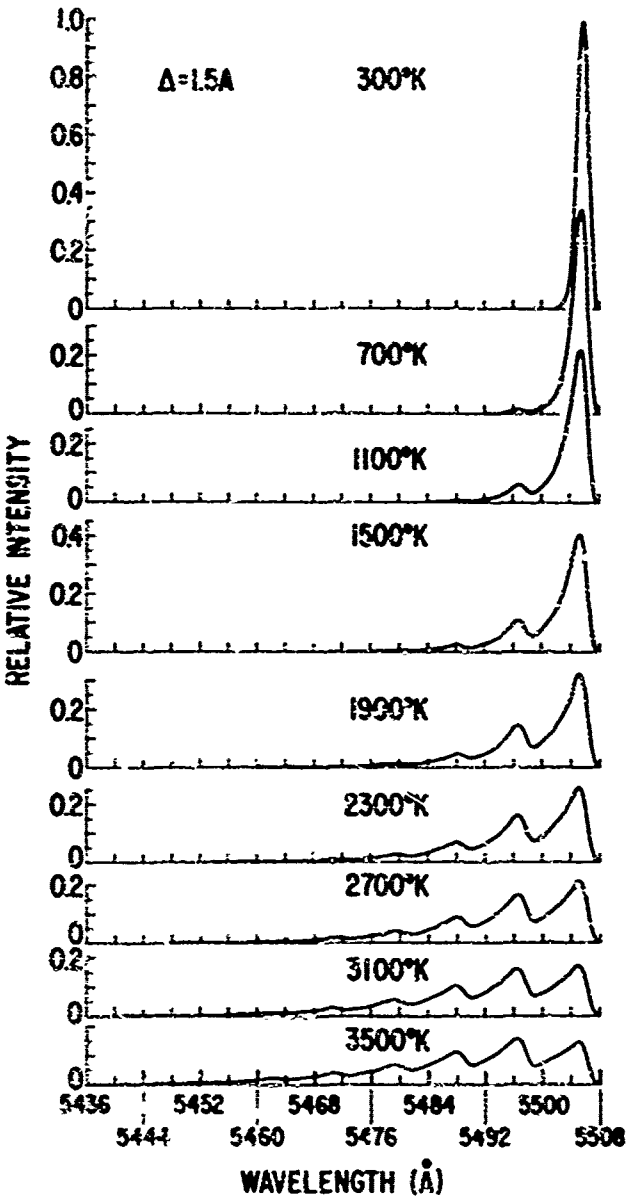

Fig. 8 Calculated Stokes Q-branch fundamental intensities for nitrogen from 300°K to 3500°K.

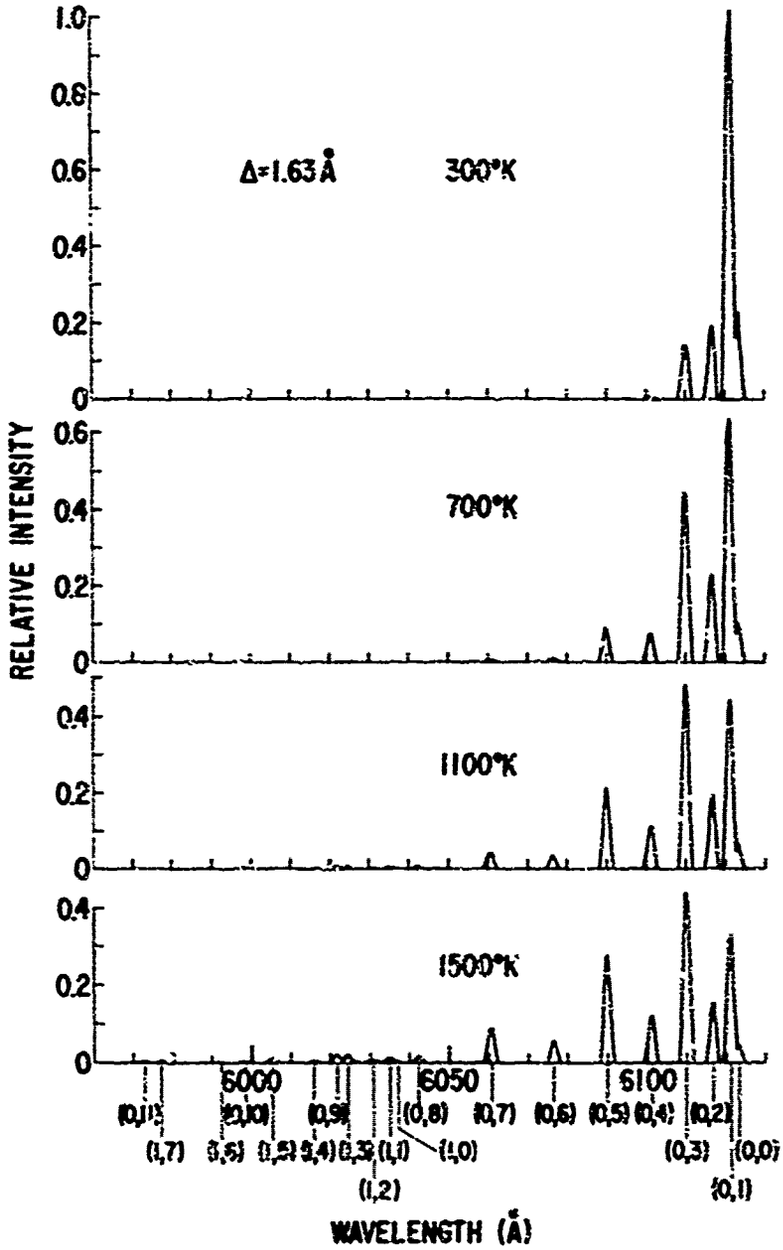

Fig. 9 Calculated Stokes Q-branch fundamental intensities for hydrogen from 300°K to 1500°K. The vertical lines along the wavelength axis indicate the positions of the various (v,J) vibration-rotation lines, where the parenthetic notation corresponds to the lower level quantum numbers.

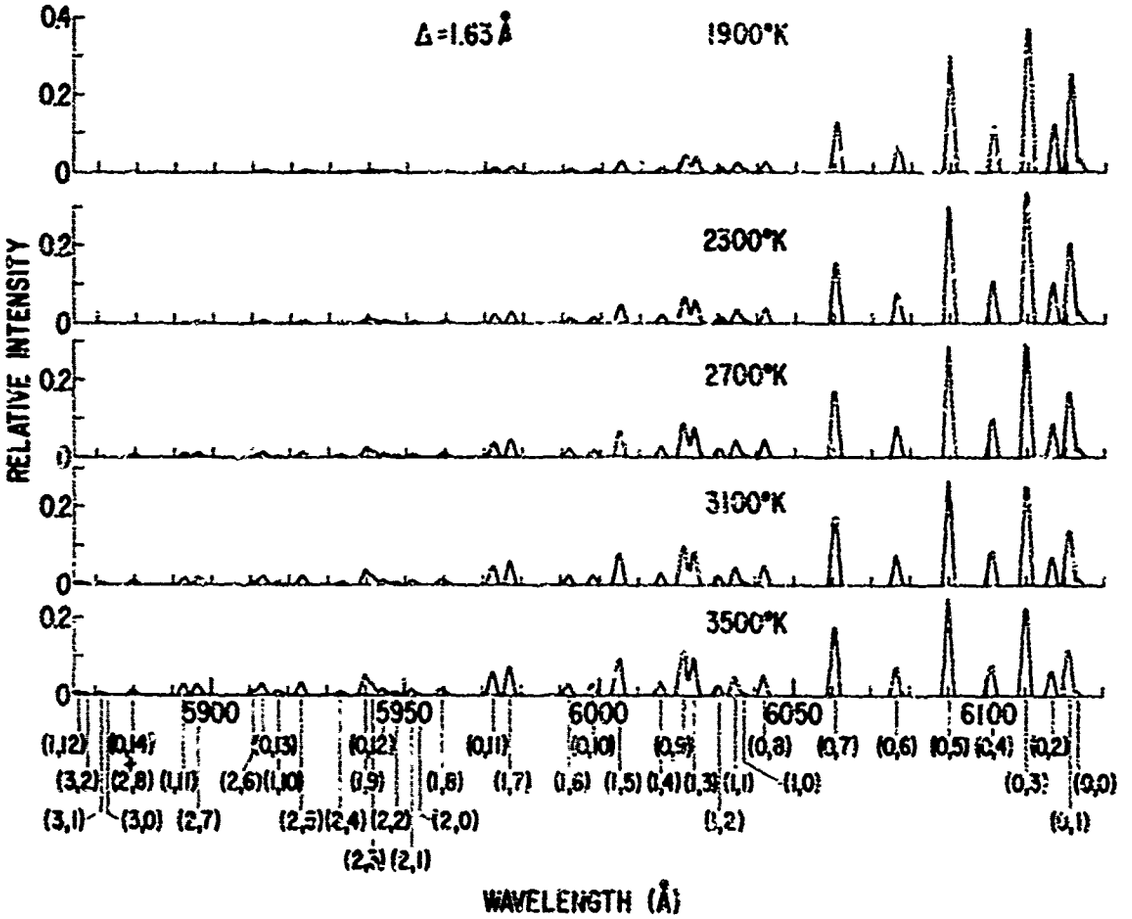

Fig. 10 Calculated Stokes Q-branch fundamental intensities for hydrogen from 1900°K to 3500°K. The vertical lines along the wavelength axis indicate the positions of the various (v,J) vibration-rotation lines, where the parenthetic notation corresponds to the lower level quantum numbers.

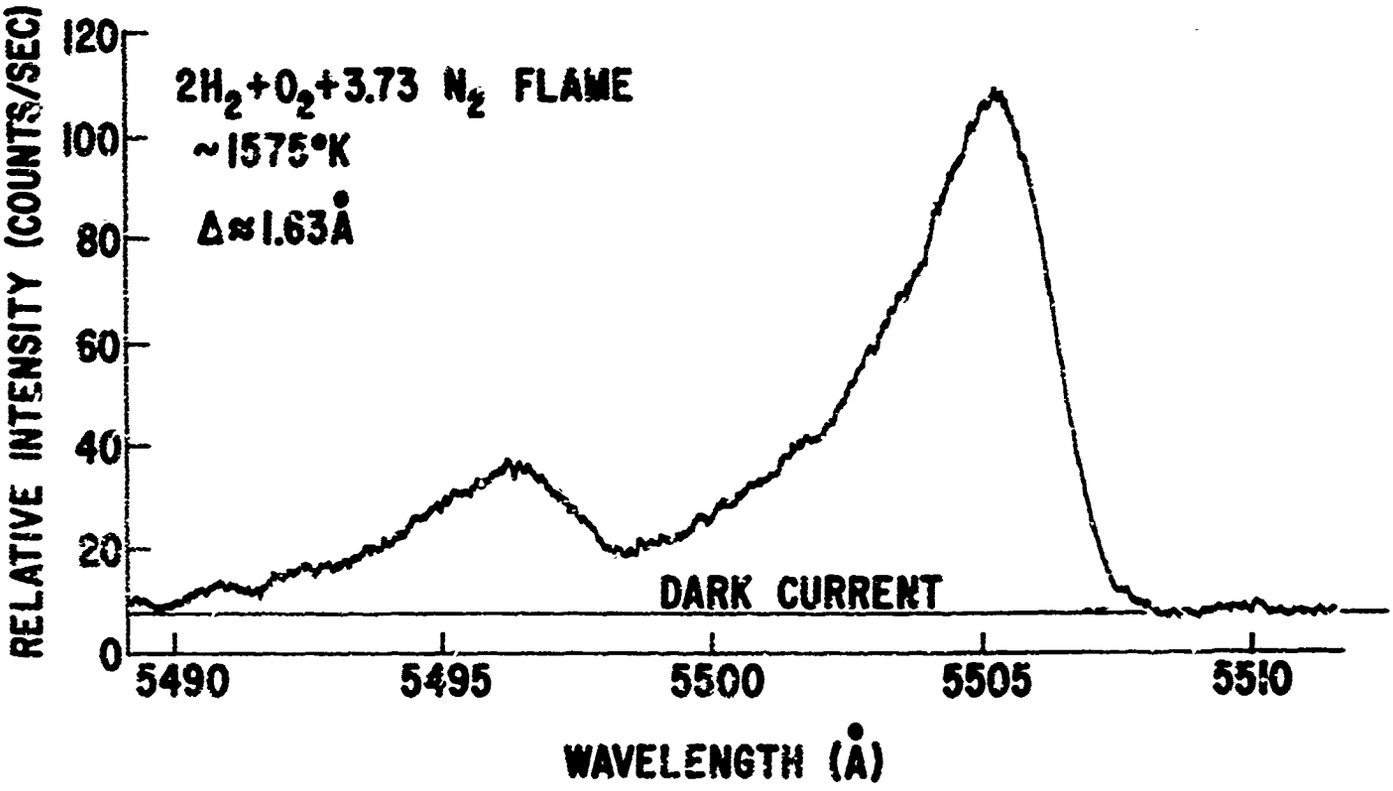

Fig. 11 Analog x-y recorder trace of Stokes vibrational Q-branch for nitrogen.

as recorded by an analog x-y recorder. The same data as recorded by paper tape data logging appears in Fig. 12. Here, the number of counts was recorded every ten seconds (i.e., every 0.02 nm for the spectrometer scan speed used).

In order to theoretically fit the experimental profile and thereby determine the nitrogen temperature, the experimental data wavelength axis was first made coincident with the proper theoretical wavelength axis by manually overlaying the experimental data on a normalized (i.e., at the ground state band peak) set of theoretical profiles. (See.Fig. 13) These profiles all have very similar long-wavelength edges, determined over this temperature range almost entirely by the monochromator slit function shape. This long-wavelength edge was therefore useful in determining the proper absolute wavelength values for the experimental data. In future work, it is contemplated to perform this axis adjustment (required by slight backlash in the monochromator scanning mechanism) automatically through use of a computer-fit of the long-wavelength edge utilizing an initially assumed approximate temperature.

The next step in the determination of temperature involved a calculation based upon the ratio of intensities recorded by the monochromator in the vicinity of the peaks of the first upper state band and the ground state band. (See Fig. 14) Each of these bandpasses was 0.18 nm wide, and contained ten data points. The theoretical ratio shown in Fig. 14 was stored as a data file in the computer, and the computer-determined peak ratio for the experimental data could then be compared to this data file, resulting in a determination of temperature. The theoretical ratio of peak bandpass intensities is

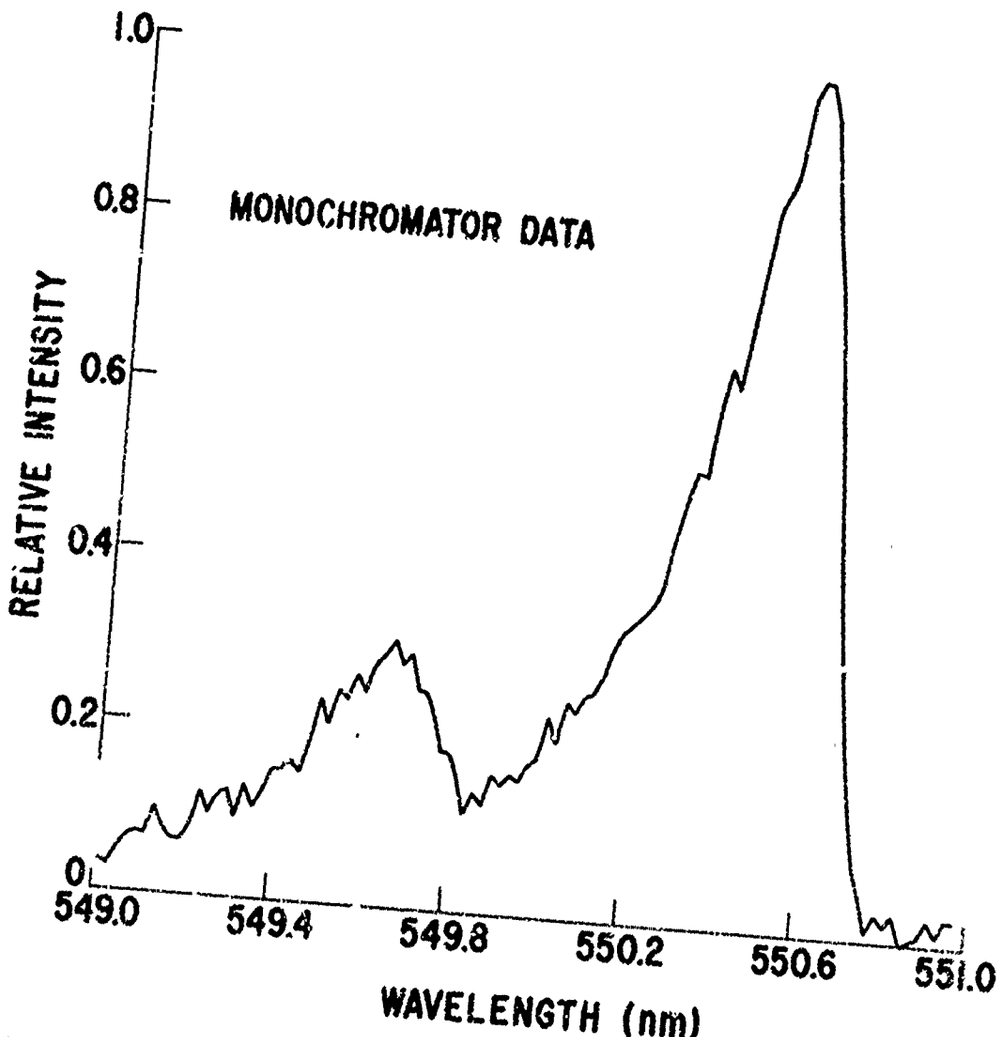

Fig. 12 Stokes vibrational Q-branch for nitrogen recorded by data logging in 0.02 nm intervals corresponding to the same conditions as for Fig. 11.

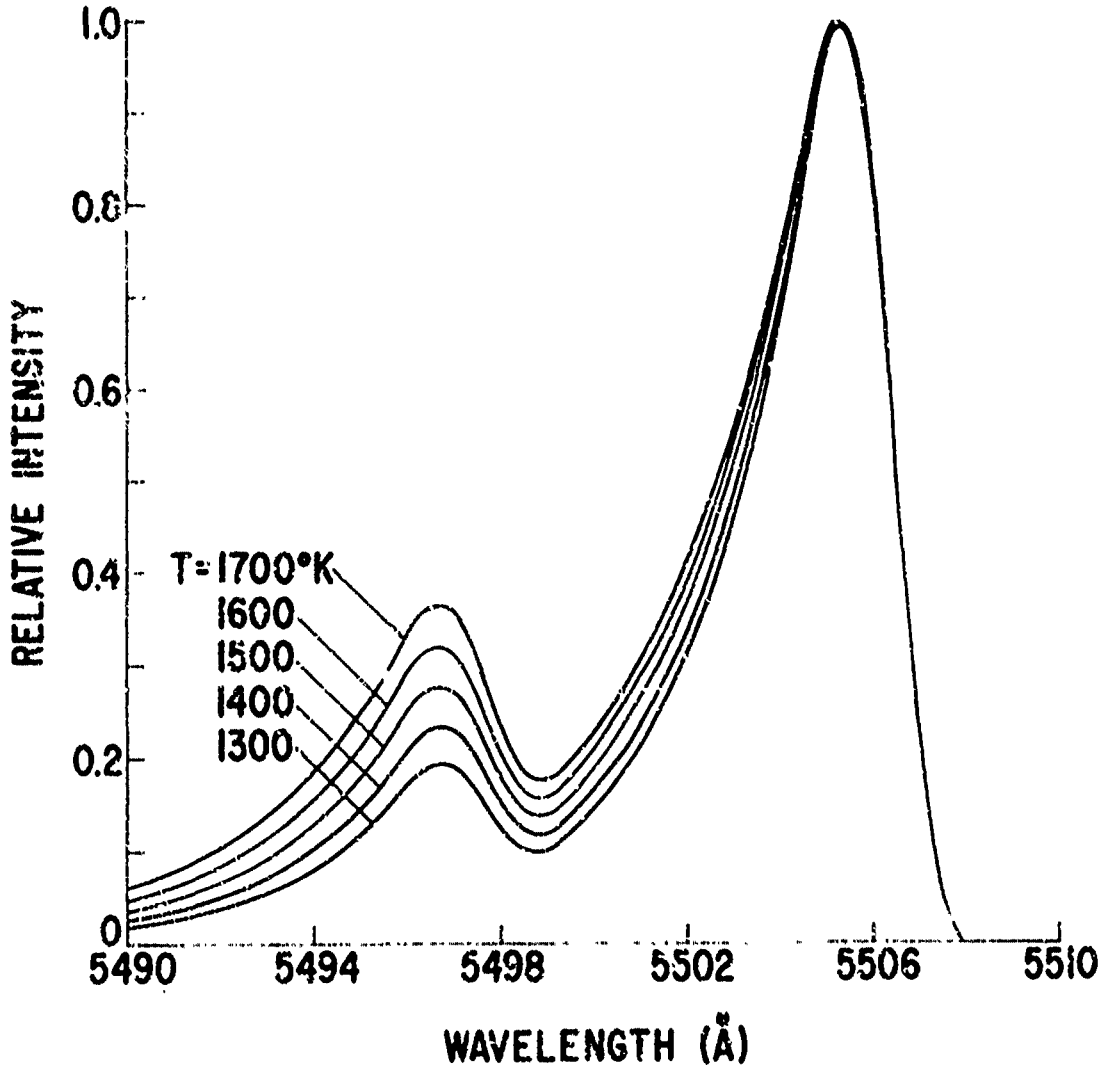

Fig. 13 Theoretically-calculated Stokes vibrational Q-branches from 1300°K to 1700°K, with peak ground state band intensities all normalized to unity. The sensitivity of those profiles to temperature for experimental profile-fitting procedures is illustrated by this set of curves.

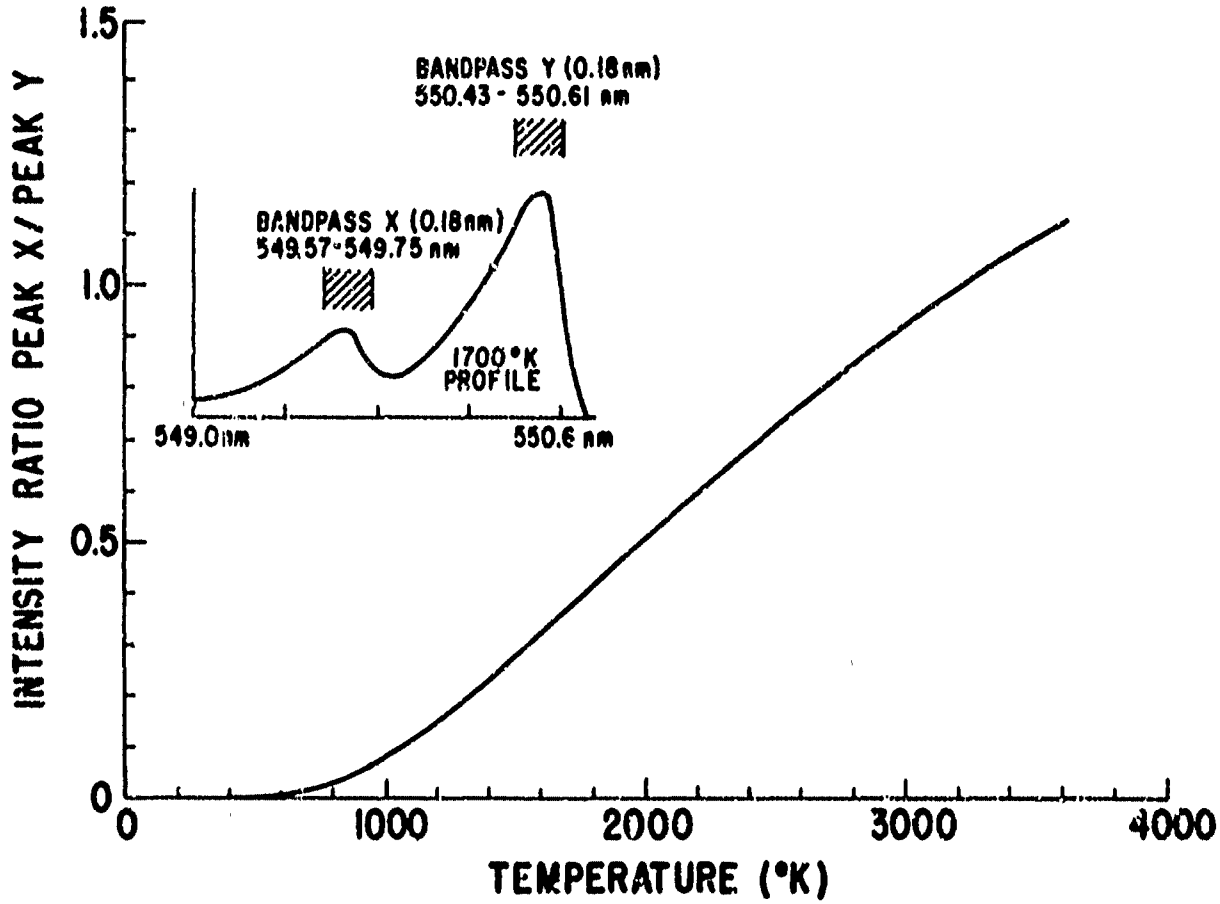

Fig. 14 Intensity ratio as a function of temperature for 0.18 nm rectangular bandpasses in the spectral vicinity of the first upper state band and ground state band for the nitrogen Stokes vibrational Q-branch.

also shown in Fig. 15 over a smaller temperature range applicable to porous plug burner experiments. This ratio is almost exactly linear over this range of temperature. For the flame studied here, the temperature determined by this procedure was 1546°K.

The final step in temperature measurement involved a least-square computer curve-fitting treatment of the experimental data. The initial assumed temperature for this procedure was that determined from the band peak ratio method just described. The minimum least-square deviation was then searched for by the computer as a function of temperature, and the temperature corresponding to this minimum deviation determined thereby to the nearest 1°K.

This method of temperature determination has a basic shortcoming in that it is based upon use of raw monochromator data, to which the peak of each trial theoretical profile must be normalized. Thus, any noise "spike" of other random inaccuracy in the ground state band peak intensity can cause a substantial distortion of the curve fitting procedure by producing a "false" normalization, with subsequent vertical stretching or squeezing of the profile. This problem can be circumvented by the averaging of adjacent data points, which can be performed by the computer to produce a new "smoothed" experimental data file. A program has been written to accomplish this smoothing by averaging over any odd number of data points in an equally-weighted fashion. Thus, for a three-point data average at wavelength λ, with δ equal to the spectral interval between data points, the new intensity at λ corresponds to (1/3) times the originally-encoded intensities at $\lambda-\delta$, λ, and $\lambda+\delta$.

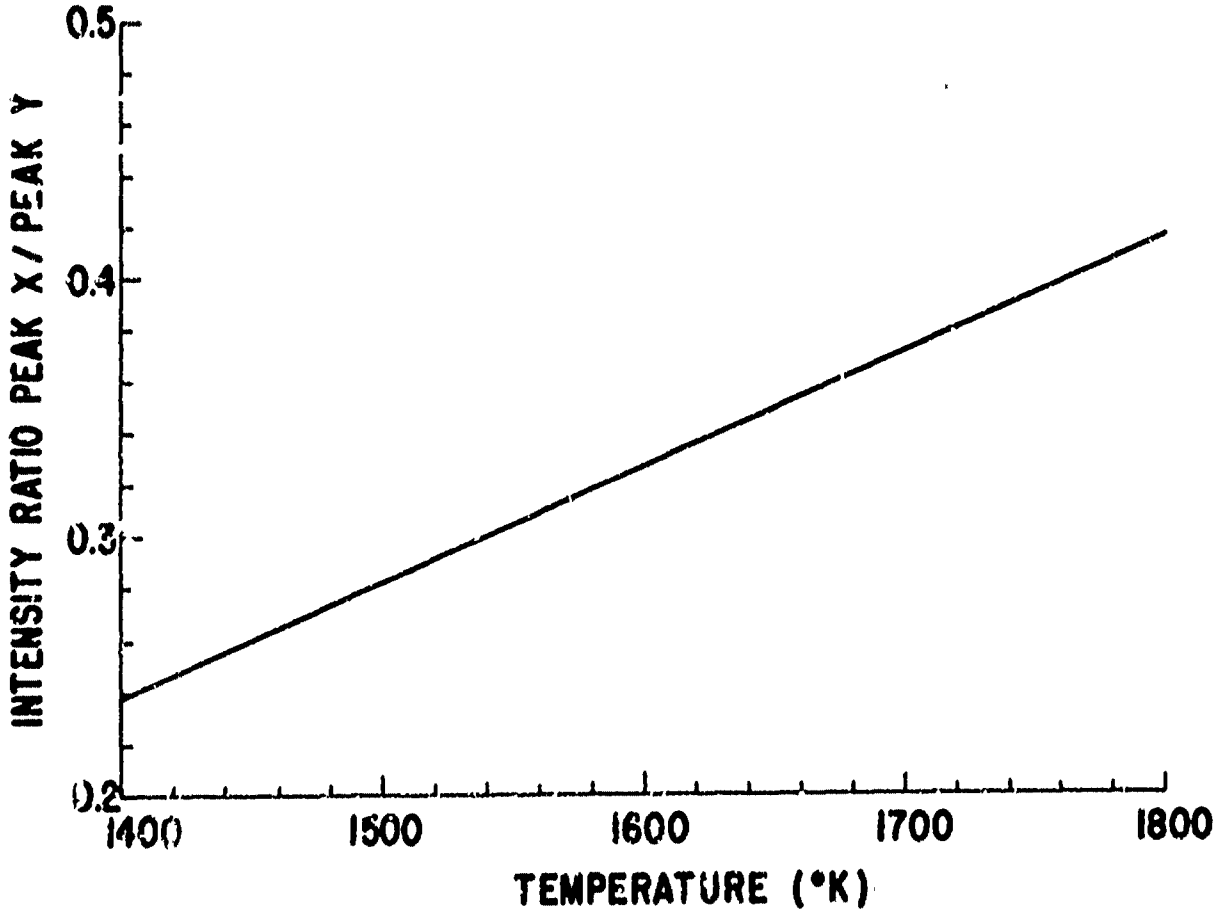

Fig. 15 Intensity ratio as a function of temperature for 0.18 nm rectangular bandpasses in the spectral vicinity of the first upper state band and ground state band for the nitrogen Stokes vibrational Q-branch. The intensity ratio over the temperature range shown here is almost exactly linear with temperature.

In turn, this method of data smoothing has a clear shortcoming in that it also distorts the overall profile in the vicinity of sharp, nonlinear changes of intensity. Thus, a compromise approach is dictated, in which data smoothing is accomplished over an optimized spectral interval. This has been done for the data shown in Fig. 12, for which three-point, five-point, and seven-point data averages were taken. In Fig. 16 is shown the three-point averaged data, while the five-point averaged data is shown in Fig. 17 along with a theoretically-calculated profile computed at T = 1546°K (the temperature determined by the peak ratio method described previously) and normalized to the peak of the data-averaged experimental curve.

In the table contained in Fig. 18 is shown the results of the least square computer fitting procedure for the raw monochromator data, and the three-point, five-point, and seven-point averaged data. The temperature corresponding to the minimum deviation [i.e., T(min), corresponding to the minimum value of Σ(deviations)] for each treatment of the data increases here as the amount of data averaging increases. It is easily seen that as the data averaging is increased excessively, the spectral profile is "flattened out", resulting in an appearance closer to that corresponding to higher temperatures.

As a working criterion for determining the optimum amount of data averaging, the procedure chosen utilized the smallest "minimum value of Σ(deviations)". As may be seen in the table contained in Fig. 18, the smallest value occurred for the five-point data average and, accordingly, this was chosen as the appropriate treatment for the data. The graph shown in Fig. 18 illustrates the variation of Σ(deviations) with temperature for the five-point data average, and indicates resultant best fit at a value of T(min) = 1538°K.

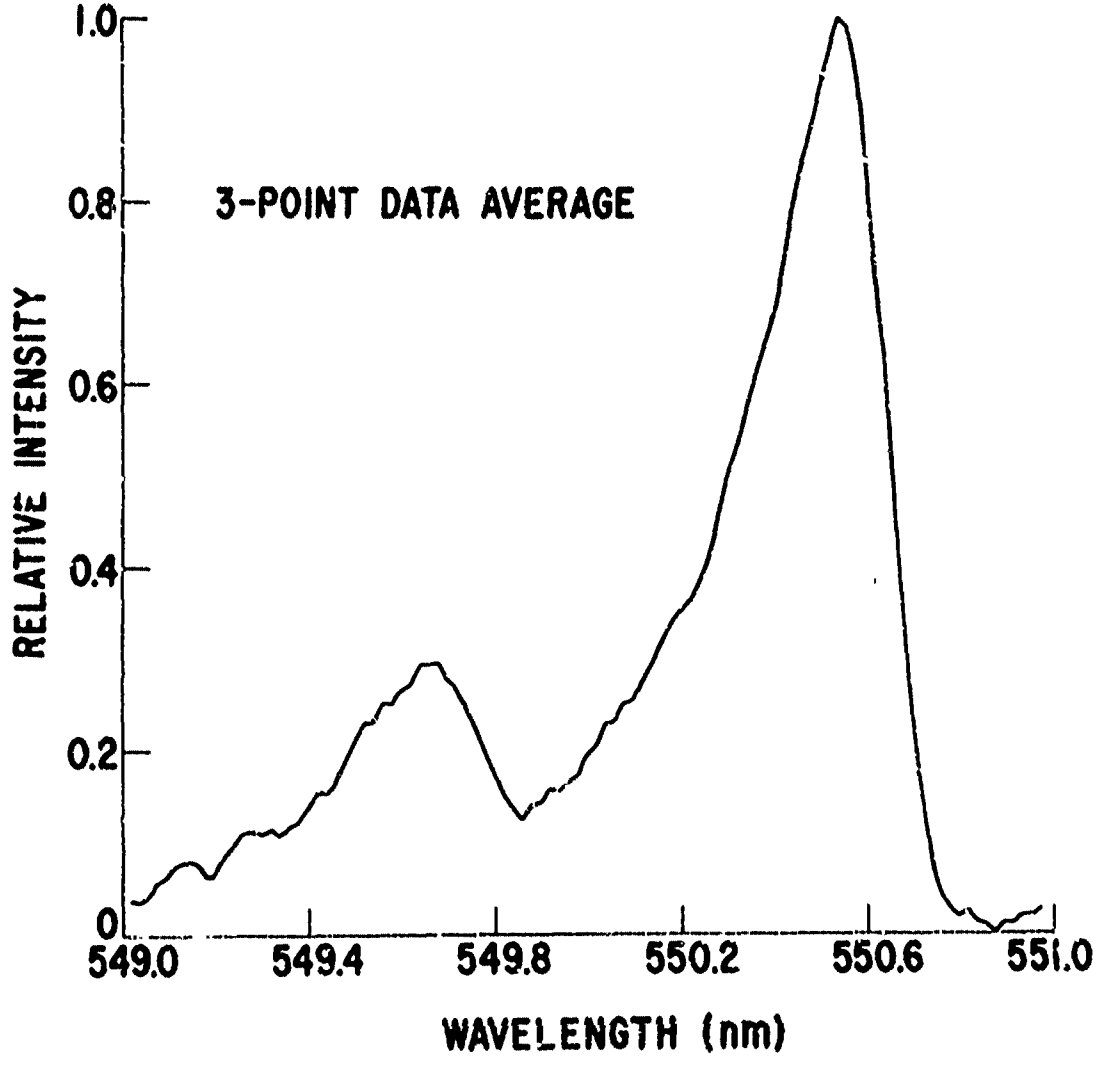

Fig. 16 Three-point data-averaged Stokes vibrational Q-branch profile for nitrogen, obtained from the raw data of Fig. 12

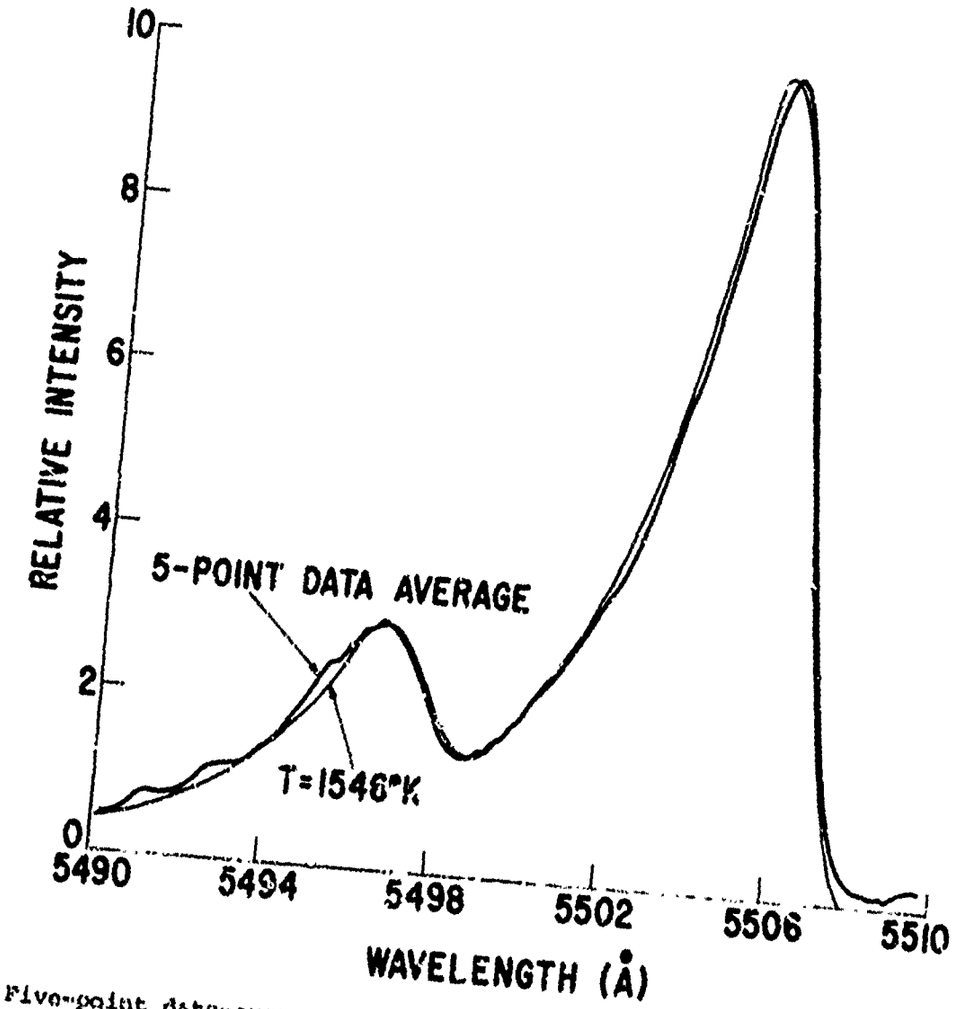

Fig. 17 Five-point data-averaged Stokes vibrational Q-branch profile for nitrogen, obtained from the raw data of Fig. 12. Also shown is a theoretically-calculated profile for 1546°K normalized to the experimental peak ground state band intensity.

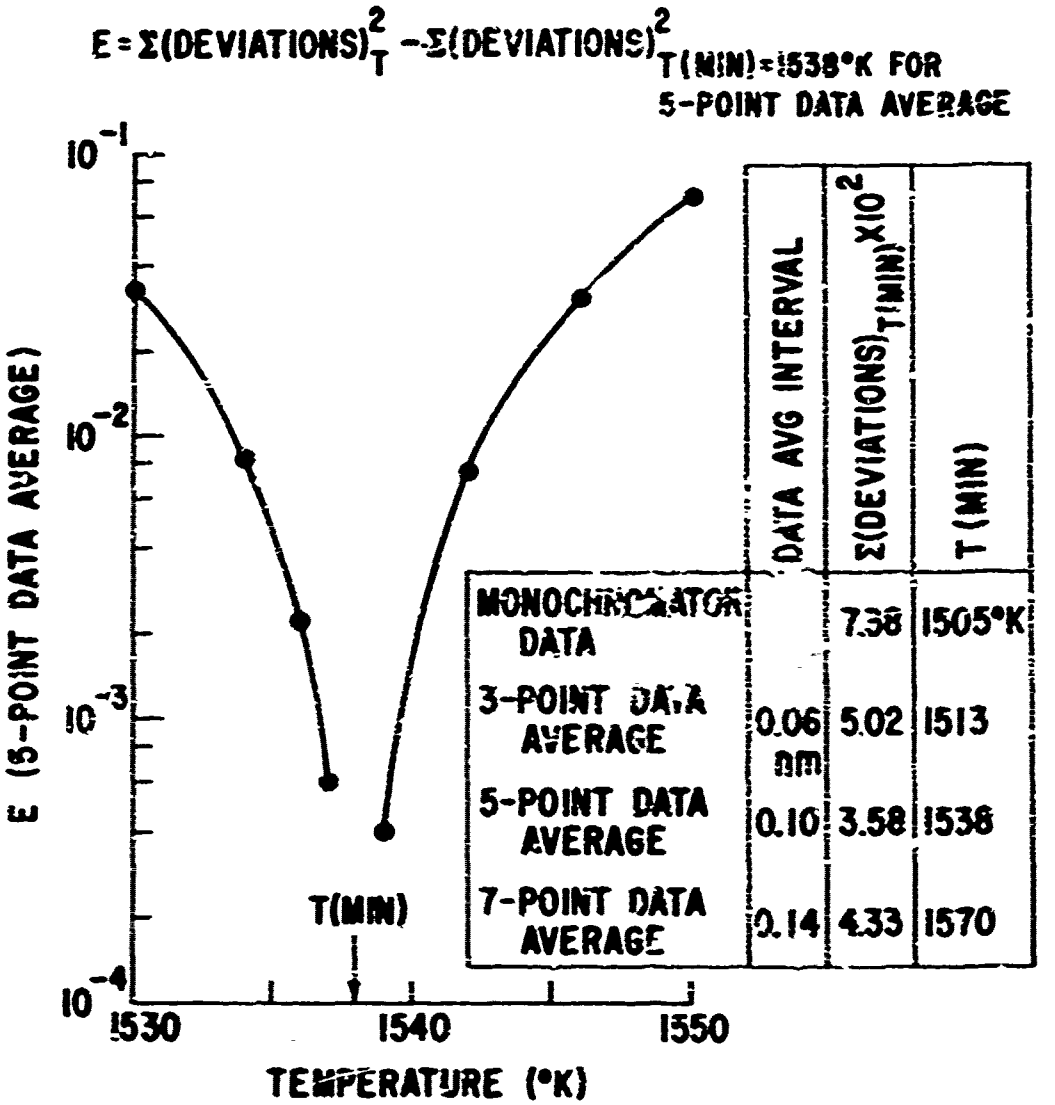

Fig. 18 Table. Summary of temperatures T(min.) corresponding to the minimum value of Σ(deviations) for the least square profile-fitting procedure, computed for the raw monochromator data and for three cases of data averaging. Figure. Variation of Σ(deviations) as a function of temperature for the five-point data-averaged profile.

Summarizing our findings for the accurate determination of flame temperature for nitrogen:

1. Sensitivity for measurement by averaged band peak ratios is shown in Figs. 14 and 15.

2. Sensitivity for curve fitting is illustrated by the set of normalized curves shown in Fig. 13.

3. The temperature measured by the band peak ratio was 1546°K.

4. The temperature measured by the best (five-point) data-averaged computer profile fit was 1538°K.

5. The temperature indicated by the fine wire thermocouple was 1525°K plus an approximate 50°K radiative correction, for an estimated flame temperature of 1575°K.

Current agreement between the peak intensity ratio method and the curve fitting method is about ½%. It is intended to pursue these techniques to determine their limiting accuracies, with an emphasis on variations of the methods which produce good accuracy with a minimum of complexity in the data handling. Thus, the trend is toward utilizing the full profile fit as a "calibration" of the simple band ratio method. This latter method can be made more accurate by utilizing more than the presently-used two bandpasses.

The full profile-fitting method will retain its utility for investigations of non-thermal equilibrium signatures. It will be particularly useful when neither vibrational nor rotational equilibrium exists. In this case, a deconvolution of the Raman scattering profile results in a determination of the relative populations of the various vibrational and rotational levels.

It is stressed here that Raman scattering signatures are direct measures of the relative populations of the molecular internal modes, and, for equilibrium situations, these relative populations correspond to the fundamental definition of temperature. Thus, it is contemplated that this form of temperature diagnostics has the potential for becoming the most fundamentally accurate scheme for non-perturbing, three-dimensional measurements.

V. Experimental Results for Hydrogen

The nitrogen data discussed in Section IV were taken with a view toward high-accuracy temperature diagnostics. The hydrogen data discussed in this section were taken in order to investigate the different type of Raman vibrational signature produced by a very light molecule, and were not intended for accurate temperature measurements.

The profile of hydrogen obtained from a four-times-stoichiometric hydrogen-air flame at a thermocouple-measured temperature of about 1390°K (corrected roughly for radiative losses) is shown in Fig. 19 as observed through use of an analog x-y recorder. The first four rotational lines of the Stokes vibrational Q-branch are identified. (For purposes of comparison, see Fig. 9 for a theoretically-calculated curve of the entire Q-branch at 1500°K.) In Fig. 20 is shown the same data as obtained from the paper tape data logger, where the trace shown as the solid curve contains the Raman scattering data, and the dashed curve is a subsequently-run emission spectrum of this luminous flame. The emission spectrum has been subtracted from the emission-plus-scattering spectrum in Fig. 21, and a theoretically-calculated (dashed) curve added for hydrogen at 1400°K. Keeping the J = 3

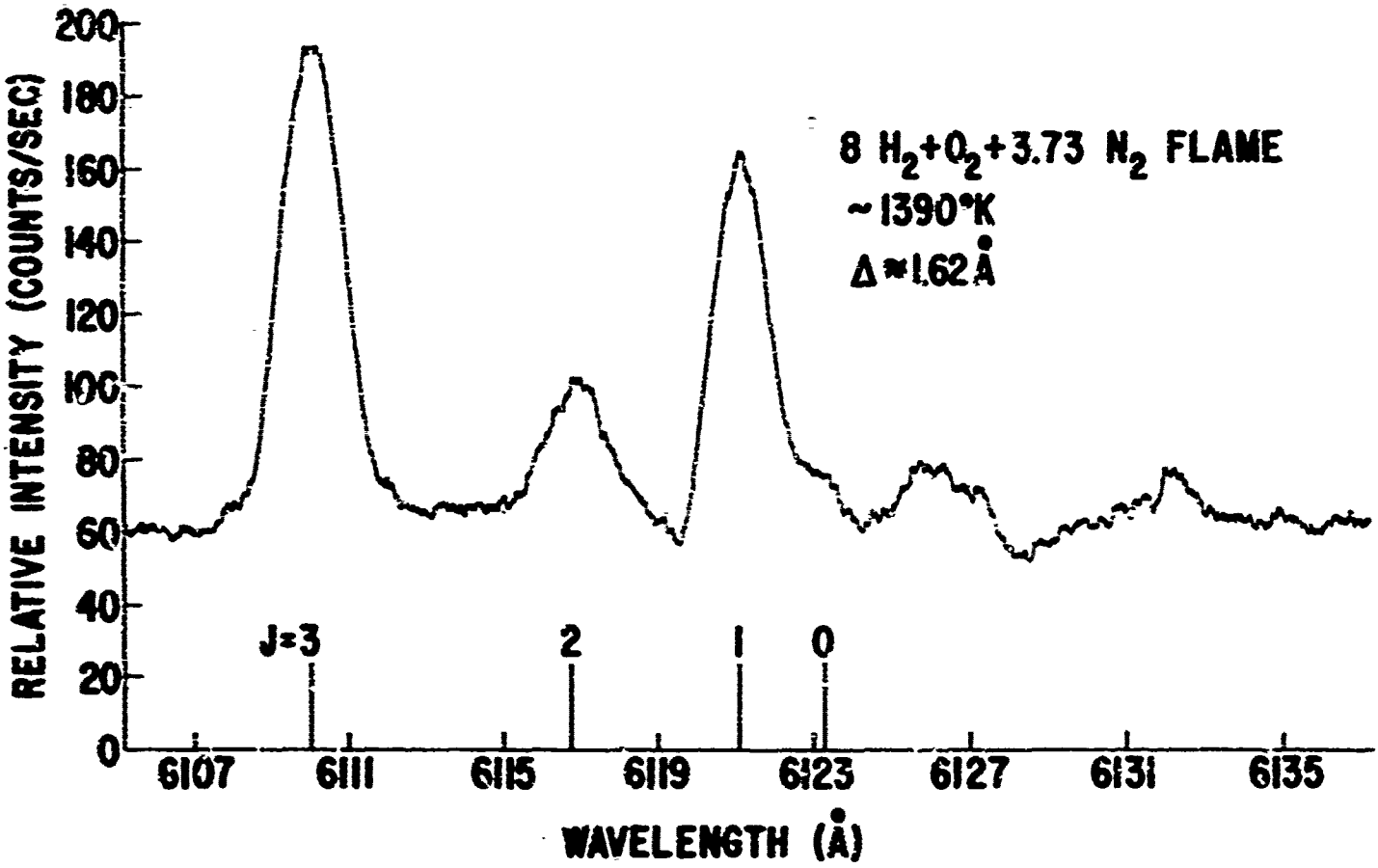

Fig. 19 Analog x-y recorder trace of first few rotational lines of Stokes vibrational Q-branch for hydrogen.

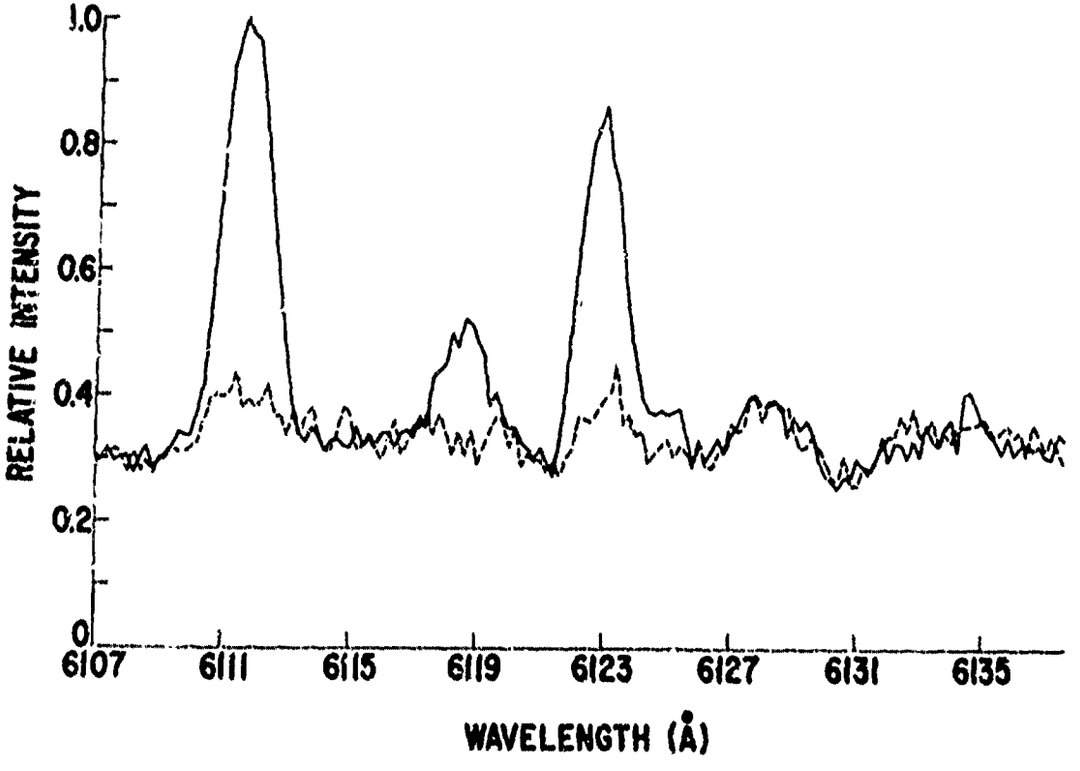

Fig. 20 Experimental Stokes Q-branch fundamental profile (solid curve) for hydrogen for four-times-stoichiometric hydrogen-air flame ($8H_2 + O_2 + 3.73\ N_2$). The dashed curve is a subsequently-run emission spectrum for this slightly luminous flame. The thermocouple-measured temperature was approximately 1390°K, and the spectral slit width $\Delta = 1.62$Å.

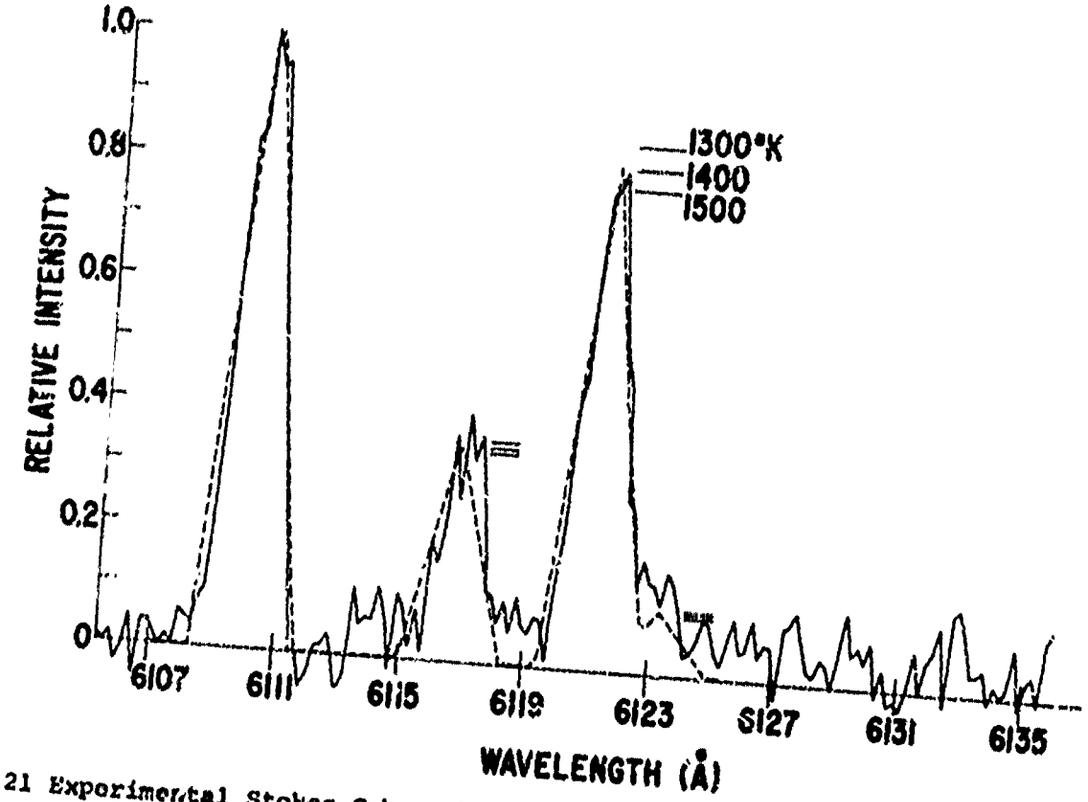

Fig. 21 Experimental Stokes Q-branch fundamental profile (solid curve) for hydrogen for the conditions of Fig. 20. Here, the emission spectrum (dashed curve of Fig. 20) has been subtracted from the scattering-plus-emission spectrum (solid curve of Fig. 20). A theoretically-calculated profile for hydrogen at 1400°K (dashed curve) has been added, and has been normalized to the experimental peak intensity for the J = 3 line. Keeping the peak intensities normalized for the J = 3 line, profiles were calculated at 1300°K and 1500°K. The corresponding peak intensities of the J = 0, 1, and 2 lines are indicated here by horizontal bars.

calculated peak intensity normalized to the experimental peak intensity. profiles were also calculated for other temperatures. The peak values for $J = 0$, 1, and 2 at 1300°K, 1400°K, and 1500°K are indicated by the appropriate horizontal lines in this figure. The accuracy of temperature measurements for the hydrogen data shown here is not good for two main reasons: (1) the flame is somewhat unsteady and non-isothermal, and (2) ratios of the vibration-rotation line intensities shown here are not particularly sensitive to the temperature over this temperature range. Other ratios utilizing higher rotational lines are more sensitive for this range. However, the profile presented here is indicative of the type of data and the required treatment for temperature estimates utilizing light molecules. The relatively wide spectral intervals between vibration-rotation lines for these molecules suggests that, with proper choice of bandpass, interference filters could eventually be used for temperature determinations with greater ease than would be the case for heavier molecules.

VI. Conclusion

The vibrational Raman signatures for nitrogen and hydrogen have been studied for hydrogen-air flames produced on a water-cooled porous plug burner. Accurate determinations of temperature have been performed utilizing the nitrogen data from a band ratio method and from a total profile-fitting procedure. These determinations as well as various other theoretical predictions have made wide use of computer calculation techniques. The temperatures found from the Raman methods agreed with each other to within ½ percent, and agreed with an independently measured temperature utilizing a fine

wire thermocouple (only roughly corrected for radiative losses) to within 2%.

The hydrogen signature has been fitted to theoretical predictions for low-lying rotational lines, and exhibits a spread-out structure which may be particularly useful for temperature diagnostics. Additional equipment has been assembled for improvements in the spectroscopic, combustion, temperature-measurement, and data acquisition and reduction aspects of the experimental program. These will be used in further study of laser Raman probes for combustion diagnostics.

Acknowlegements

The author is grateful to Dr. John Moore for thermocouple fabrication, to Mr. Harry Horton for his contributions to thermocouple temperature and gas flow measurements, and to Mr. Frank Haller for computer programming. Some of the preliminary material reported here was presented by M. Lapp at the Third International Conference on Raman Spectroscopy,[4] Reims, France, 1972.

References

1. M. Lapp, L.M. Goldman, and C.M. Penney, Science 175, 1112 (1972).

2. W.E. Kaskan, Sixth Symposium (International) on Combustion (Reinhold, New York, 1957), pp. 134-143.

3. A.G. Gaydon, Spectroscopy of Flames (Chapman and Hall, London, 1957), pp. 79, 90, and 241.

4. The conference proceedings will be published as Advances in Laser Raman Spectroscopy, Vol. 1 in 1973 by Heyden and Son Ltd., London.

Appendix 1

Raman Scattering from Flames

M. Lapp, L.M. Goldman, and C.M. Penney

Science 175 1112 (1972)

SCIENCE

Raman Scattering from Flames

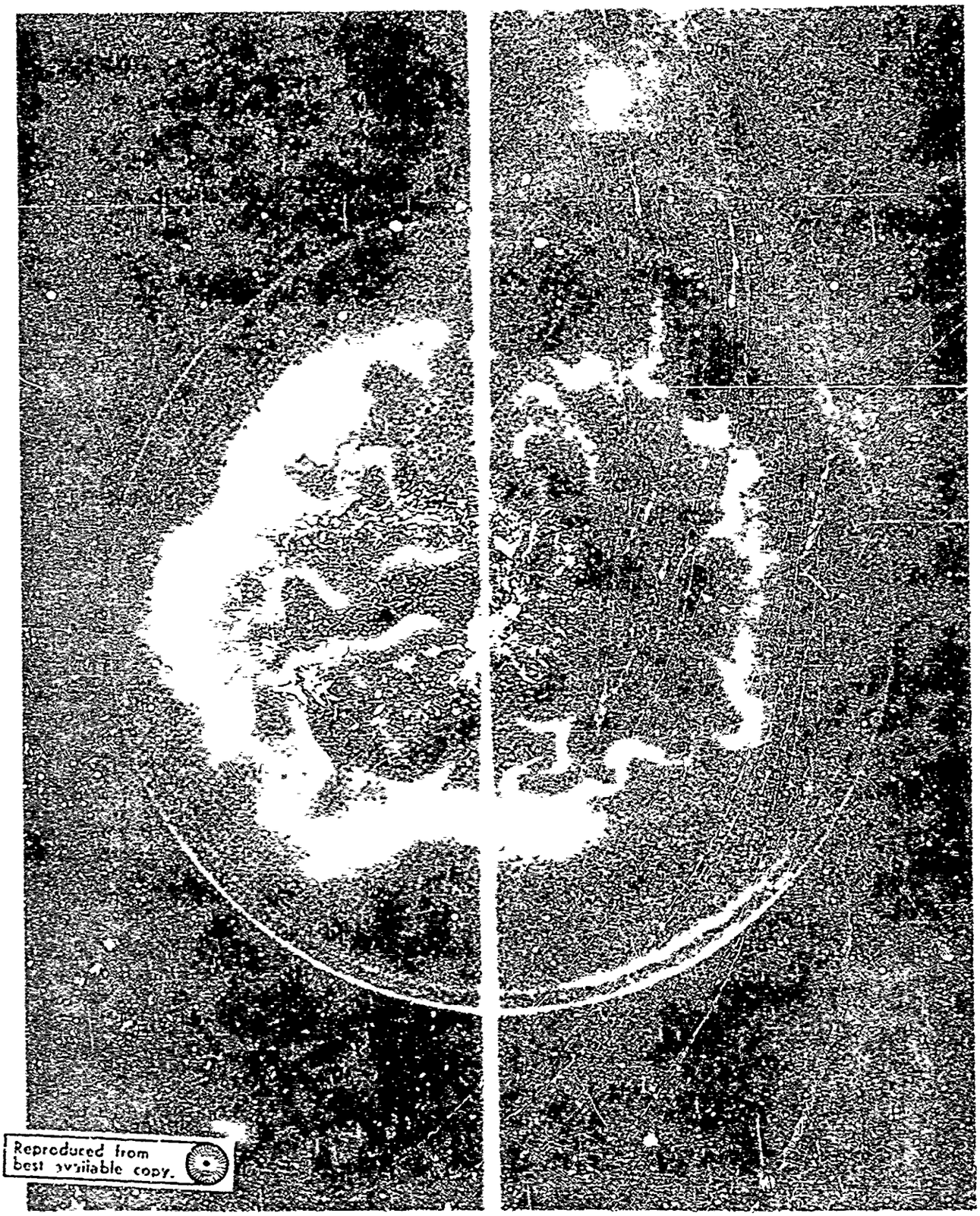

COVER

End view of a flame burning horizontally on a porous plug burner (2.5 centimeters in diameter). A focused laser beam is passing vertically through the flame for Raman scattering experiments. See page 1112. [S. W. Blanchard, Graphics Unit, General Electric Co., Corporate Research and Development, Schenectady, New York]

Raman Scattering from Flames

Abstract. *Laser Raman scattering data for nitrogen, oxygen, and water vapor have been obtained from hydrogen-air and hydrogen-oxygen flames. The resulting ground-state and upper-state vibrational bands exhibit strong asymmetrical broadening. Experimental spectral profiles have been fitted theoretically to give a new measurement technique for the determination of rotational and vibrational excitation temperatures.*

We report here observations of vibrational Raman scattering from flame gases. One motivation for these observations is that Raman scattering can provide spatially resolved measurements of the concentration and the vibrational and rotational excitation temperatures of flame constituents. This capability should prove to be of substantial use in the diagnostics of nonequilibrium as well as equilibrium phenomena.

The work presented here is focused upon the observation of temperature-dependent effects in the spectral distribution of the Stokes Q-branch vibrational scattering. These effects arise predominantly from the vibration-rotation interaction and from significant populations of excited vibrational levels. From these excited levels originate upper-state bands (*1*) which are usually shifted toward the blue region of the spectrum.

In Fig. 1 we show the types of fundamental vibrational Raman scattering events that may be observed in flames. Earlier Raman scattering experiments at elevated temperatures have dealt with laser heating of a vapor (*2*), with studies of species in ovens at temperatures up to 1000°C (*3*), and with a low-pressure electric discharge (*4*). We have been unable to find any earlier publications concerning Raman scattering in flames or in any systems at temperatures in excess of 1000°C.

Our initial observations were confined to Stokes bands arising from 4880-Å incident radiation from an argon ion laser (Coherent Radiation model 52B) operated for most data at 1.5 watts. The scattered light was analyzed by a double monochromator (Spex 1400-II) with 5000-Å blazed gratings. The detector was a cooled photomultiplier (RCA C31000E Quantacon) operated in the pulse-counting mode with dark current levels of about 18 counts per second for this work.

The overall experimental arrangement was designed to have the laser beam traveling along the direction of the entrance slits (that is, vertically) and focused at a position about 0.3 m from the entrance slits. The Raman-scattered radiation was collected by a multielement lens with a focal length of 75 mm. The width of the laser beam in the scattering zone was about 100 μm, and the height from which the scattered radiation was accepted (as determined by the 1-cm slit height and the image magnification factor of 2) was about 5 mm. The monochromator entrance and exit slits were set to 300 μm, for which the spectral slit width was measured to be in very close agreement with the value calculated from the instrument dispersion curve. The (Rayleigh and Mie scattering) image of the laser beam at the entrance slits (as viewed by a periscope attachment behind the slits) showed no change when the flame was ignited.

The flames studied were produced on a water-cooled porous plug burner (diameter, 2.5 cm) (*5*) operated horizontally and burned into another water-cooled porous plug (of larger diameter) placed about 1.5 cm away which was, in turn, connected to a rough vacuum line. In this fashion, a stable horizontal flame at atmospheric pressure was produced which possessed the advantage of offering a scattering test zone of uniform conditions (that is, at a constant distance from the flat flame front) for a laser beam passing in the vertical direction. Scattering data for H_2O and O_2 were obtained from lean H_2-O_2 flames, whereas data for N_2 was obtained from a lean H_2-air flame. Because of the low luminosity of these flames in the spectral regions of interest, no increase in background was observed when the flames were ignited. Precise flow data were not taken, nor

were accurate independent temperature measurements made, since the major goal of this portion of our flame Raman scattering investigation was the exploration of general temperature-sensitive features of scattered bands. The temperatures actually determined from the scattering data are reasonable values for the flames used.

Although vibrational temperatures have been determined from the Stokes/anti-Stokes ratios of vibrational scattering (*2*, *6*), the same information is accessible from the Stokes scattering alone. Our initial attention to the latter is due in part to the greater sensitivity of our spectrometer and detector to the Stokes scattering. However, there is also a potential advantage to this approach which arises from the fact that temperature measurements from Stokes (or anti-Stokes) scattering alone involve a much smaller spectral range than with the corresponding measurements of Stokes/anti-Stokes ratios. Thus, in the former case it is easier to correct for the spectral variation of background, absorption, and spectrometer response.

The asymmetry of the vibrational bands is evident even at room temperature for the molecules considered here, and particularly so for H_2O. In Fig. 2B the H_2O vibrational ground-state band is shown for scattering from room temperature ambient H_2O. The greatly increased broadening toward the blue region of the spectrum under flame conditions is shown in Fig. 2A. The strong asymmetry of the N_2 and O_2 vibrational bands under flame conditions can be seen in Figs. 3 and 4. This "blue asymmetry" is explained by the fact that all the $\Delta J=0$ rotational lines corresponding to the Q-branch do not overlap each other exactly. There is a progressive shift to shorter wavelengths caused by the vibration-rotation interaction term of the energy levels for a molecule. To discuss the spectral shape and position of each band, we consider the term value $G(v,J)$ for a real diatomic molecule (*7*), including contributions from harmonic and anharmonic oscillator terms, rigid and anharmonic rotor terms, and vibration-rotation interaction terms (*8*).

$$G(v,J) = E(v,J)/hc = \omega_e(v+\tfrac{1}{2}) - \omega_e x_e(v+\tfrac{1}{2})^2 + \omega_e y_e(v+\tfrac{1}{2})^3 + (B_e - \alpha_e/2)J(J+1) - (D_e + \beta_e/2)J^2(J+1)^2 - \alpha_e v J(J+1) - \beta_e v J^2(J+1)^2 + \ldots \quad (1)$$

Here $E(v,J)$ is the energy of the level (v,J); h is Planck's constant; c is the

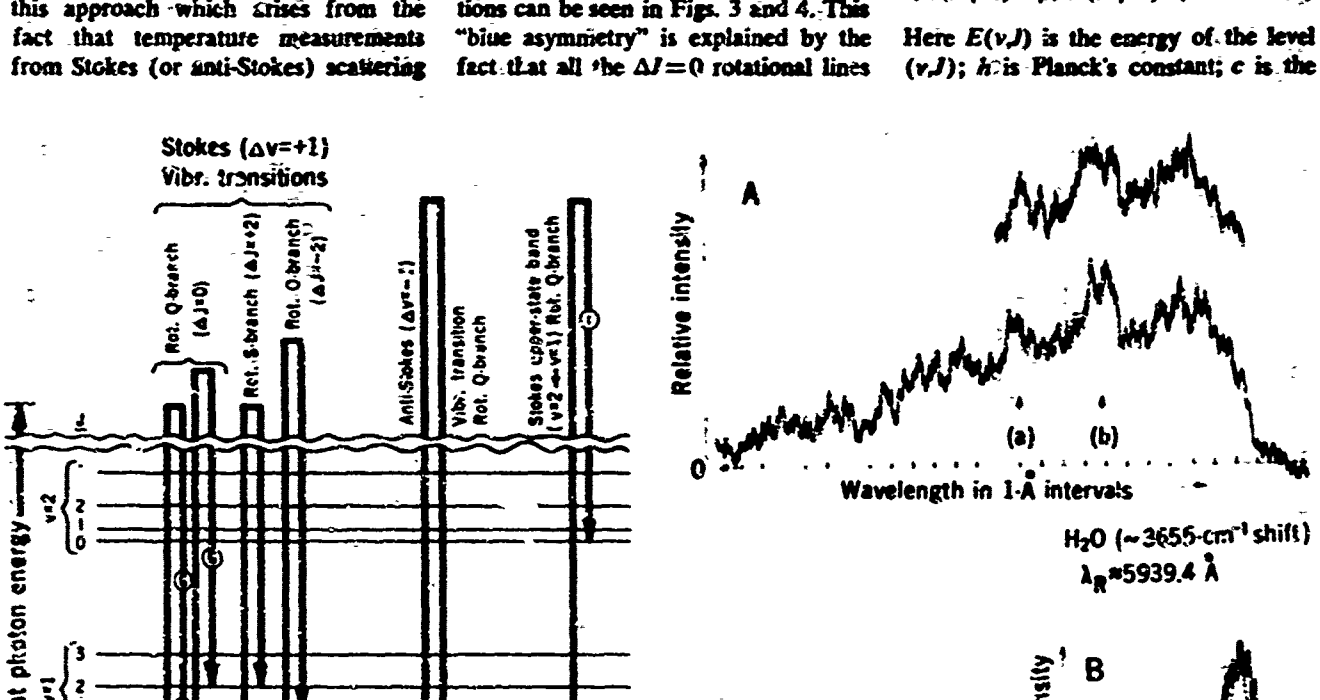

Fig. 1 (left). Schematic of some molecular transitions which contribute to fundamental vibrational Raman scattering ($\Delta v=\pm 1$). The Stokes upper-state band (circled numeral "one," at right) is associated with the molecular vibrational transition $v=1$ to $v=2$. For this transition the scattered photon energy is slightly greater than that for the ground state (that is, $v=0$ to $v=1$) Q-branch (circled letter "G") because of molecular vibrational anharmonicity. Thus, the upper-state band appears at a slightly shorter wavelength. Fig. 2 (right). (*A*) The H_2O Raman vibrational ground-state band for a lean H_2-O_2 flame. The partial segment above the full trace is a portion of another measurement shown to indicate the reproducibility of the gross features at positions (*a*) and (*b*). The latter is an upper-state band and is discussed at the end of this report. Although feature (*a*) approximately coincides with a weak Ar line at 5925 Å, experimental measurements failed to show sufficient scattering of this radiation to cause the observed signal. (*B*) The same H_2O Raman band taken in the laboratory atmosphere (295°K, 8 torr). The dashed curve is the spectrometer slit function. These curves correspond to 300-μm entrance and exit slits, for which the slit width Δ is 1.62 Å at this wavelength. The wavelength axes of these curves are indicated in a relative fashion only, since wavelength calibration lines were not included in the experiments and theoretical profiles have not yet been calculated. The wavelength $\lambda_R \sim 5934.5$ Å is slightly to the right of the peak of (*B*) (that is, at slightly longer wavelength). As an example of a case for which exact calculations are not complicated, the peak of the 295°K slit-convoluted profile for N_2 is at a wavelength about 0.3 Å less than the corresponding value of λ_R.

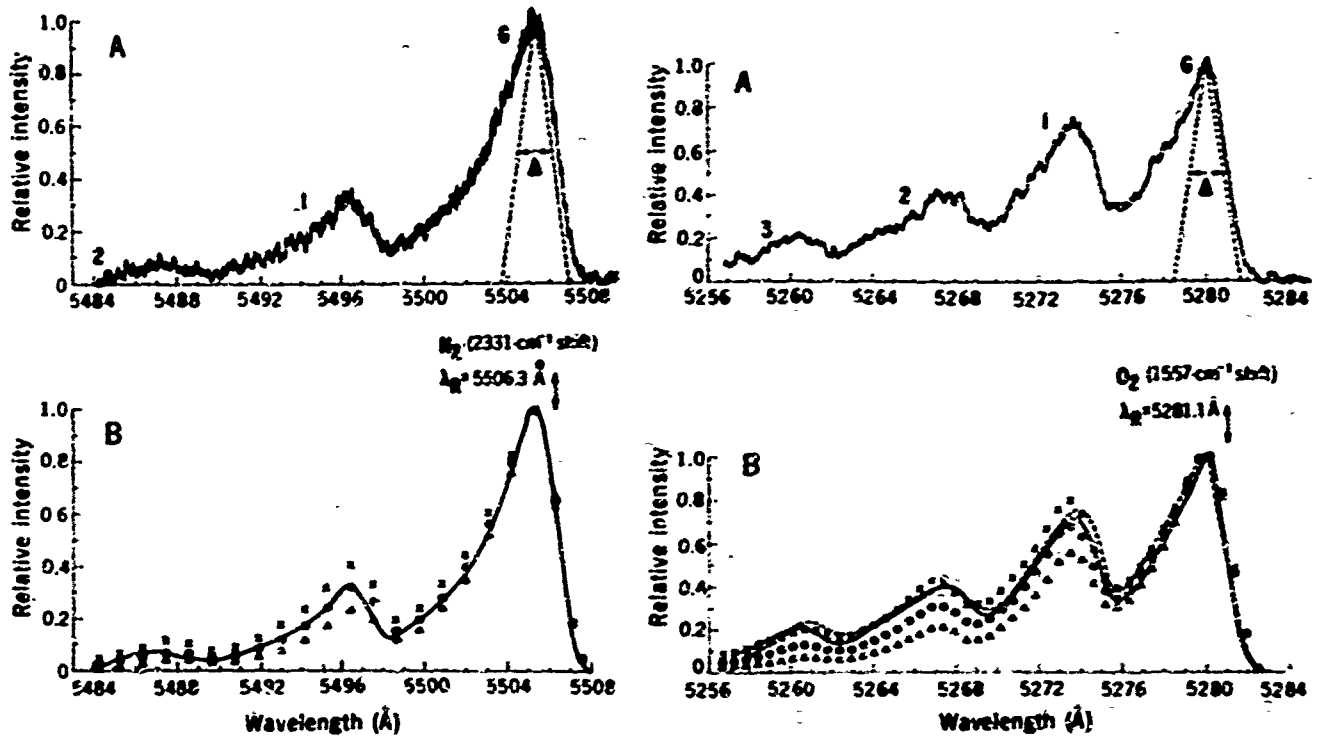

Fig. 3 (left). Raman scattering from N_2 in a lean H_2 air flame. (A) The experimental recording onto which has been superimposed the spectrometer slit function for the 300-μm entrance and exit slits used. The spectral slit width Δ is 1.63 Å. The labeling *G*, *1*, and *2* corresponds, respectively, to the ground-state Stokes vibrational Q-branch, the upper-state Q-branch ($v = 1$ to $v = 2$), and the upper-state Q-branch ($v = 2$ to $v = 3$). (B) The solid line is a tracing of the experimental curve (A), to facilitate comparison with the intensity calculated at discrete wavelengths from Eq. 3 at temperatures of 1400°K (△), 1600°K (●), and 1800°K (×). The fit of the theoretically calculated points for 1600°K with the experimental curve is quite close. Fig. 4 (right). (A) Raman scattering from O_2 in a lean H_2-O_2 flame. The general comments for Fig. 3 also apply here. However, in this case an additional upper-state band (labeled *3*) is seen. Furthermore, a tracing of a subsequent measurement under identical conditions is shown as the dashed curve in (B). These two curves give an estimate of the spread in the O_2 data, and are to be compared with the theoretically predicted shapes. An estimate of roughly 1700°K is obtained from these data.

speed of light; ω_e, $\omega_e x_e$, and $\omega_e y_e$ are vibrational constants such that $\omega_e y_e < \omega_e x_e < \omega_e$; B_e and D_e are, respectively, the rotational constants for rigid and nonrigid rotation in the equilibrium internuclear position; and α_e and β_e ($\alpha_e \ll B_e$ and $\beta_e \ll D_e$) represent vibration-rotation interactions.

The Raman shift for a fundamental vibrational band (that is, for $\Delta J = 0$ and $\Delta v = 1$) is, from Eq. 1,

$$\Delta G(v+1, J \leftarrow v, J) = \omega_e - 2\omega_e x_e(v+1) + \omega_e y_e(3v^2 + 6v + 13/4) - \alpha_e J(J+1) - \beta_e J^2(J+1)^2 + \ldots \quad (2)$$

where the vibration-rotation interaction, corresponding to the last two terms of Eq. 2, leads to the blue asymmetry for the bands. Here, β_e may be neglected, since $\beta_e \ll D_e \ll \alpha_e$.

The radiant flux *S* for a rotational line of the fundamental series ($v+1 \leftarrow v$) Stokes Raman-scattered Q-branch is given by (*9*, *10*)

$$S(v,J) \propto \frac{\eta(2J+1)(v+1)\omega_R^4 C_v}{Q_{rot} Q_{vib}} \exp\left[-\frac{hc}{kT} G(v,J)\right] \quad (3)$$

where *k* is Boltzmann's constant and ω_R is the wave number of the Raman fundamental line (*11*):

$$\omega_R = \omega_e - \Delta G(v+1, J \leftarrow v, J)$$

for which ω_e is the wave number of the incoming (laser) radiation. Here, the depolarized contribution has been neglected, and the factors associated with the cross section which are not explicitly written out are denoted by C_v. The rotational (*12*) and vibrational partition functions Q_{rot} and Q_{vib} are, respectively,

$$Q_{rot} \sim kT/2hcB_e$$

$$Q_{vib} \sim [1 - \exp(-hc\omega_e/kT)]^{-1}$$

and the factor η accounts for the effect of nuclear spin *I*. For N_2 ($I = 1$), the parity of the rotational levels is such that the symmetric levels correspond to even values of *J*, for which $\eta = 1$, whereas the antisymmetric levels correspond to odd values of *J*, for which $\eta = 2$. For O_2 ($I = 0$), the symmetric levels correspond to odd values of *J*, for which $\eta = 1$, whereas the antisymmetric levels correspond to even values of *J*, for which $\eta = 0$ (that is, the lines corresponding to even values of *J* are missing).

It is evident from Eq. 3 that the shape of each particular band (that is, a given *v*) of the fundamental series will be dependent upon the rotational temperature, and that a proper fit to an experimental profile can then serve to determine this temperature. All of the bands of the fundamental series will have somewhat similar shapes. Here, for the purposes of illustration, we consider the ground-state band. The shape of this band (that is, the *S* versus ω profile) may be calculated from Eq. 3 which, for a fixed temperature, becomes

$$S(0,J) \propto (2J+1)\omega_R^4 \times \exp[-hcB_e J(J+1)/kT]$$

with

$$\omega_R \sim \omega_e - \omega_0 + 2\omega_e x_e + \omega_e J(J+1)$$

where only those terms of quantitative significance which contribute to the relative band shape have been retained. The partition functions provide only a

temperature-dependent scale factor for Eq. 3, and so are not of concern for profile fitting.

The experiments reported here corresponded with reasonable certainty to equilibrium populations for the vibrational and rotational energy levels. However, for situations in which equilibrium is not expected, the temperature factors appearing in the exponent of Eq. 3 can be denoted as values of T_{vib} or T_{rot} associated with particular energy levels, and the vibrational and rotational excitation temperatures corresponding to these degrees of freedom can therefore be determined. In general, the relative peak value or integrated intensity of each successive band indicates the vibrational temperature, whereas the shape (that is, blue asymmetry) of each band determines the rotational temperature. Thus, if nonequilibrium is suspected, separate fits to the shape of each band should be made. In this fashion, different vibrational and rotational excitation temperatures can be associated with each internal mode. This method should complement the well-studied OH emission and absorption techniques for the measurement of excitation temperatures, which have been applied to flames with success (*13*); conversely, this method might serve to determine anharmonic terms for species that have not yet been well studied (*14*).

For the case where equilibrium exists, relative values of $S(v,J)$ can be calculated as a function of wavelength over the entire spectral extent of the scattered bands for various temperatures and the results fitted to experimental curves. This has been done (*13*) for N_2 and O_2 in Figs. 3 and 4, with the result that the N_2 data closely fit 1600°K and the O_2 data roughly fit 1700°K. These values are reasonable for the flames used. We believe that these results demonstrate the utility of this Raman scattering method for the determination of flame temperatures, as well as for temperatures in a variety of other experimental and practical areas.

For H_2O, the analytical results are considerably more complicated since the calculations involve asymmetric top energy levels (*16*). However, if we consider only the purely vibrational contributions to the energy levels for an anharmonic nonlinear triatomic molecule (*17*), we can investigate in a qualitative fashion the lowest possible upper-state bands, where we use the notation (v_1,v_2,v_3) to denote the vibrational quantum numbers for the three fundamental vibrational modes. The band corresponding to the transition (1,1,0)←(0,1,0) is the most likely to be observed, since it arises from the population of the lowest excited vibrational level ($v_2=1$, 0.20 ev above the ground state). The separation $\delta\lambda$ between this upper-state band and the ground-state band (for no rotation) is $-x_{12}$, where x_{12} is the coefficient of the $(v_1+\frac{1}{2})(v_2+\frac{1}{2})$ term in the energy level expression. For H_2O, x_{12} is -20.0 cm^{-1} and $\delta\lambda$ corresponds to a blue shift of 7.05 Å for incident 4880-Å radiation. This shift closely coincides with the position of feature (*b*) in Fig. 2A (since λ_N is located slightly to the right of the peak of the Raman scattering curve in Fig. 2B). Thus, we have evidence of an appreciable population of the H_2O $v_2=1$ level for the flame studied. More importantly, this result demonstrates the potential ability of Raman scattering measurements for polyatomic molecules.

In this report we have concentrated on temperature measurements. However, there is also substantial interest in the use of Raman scattering as a constituency probe in flames and other systems. One important point concerning such measurements is illustrated by the foregoing results. For systems wherein significant vibrational and rotational excitation occurs, temperature-dependent calculations, such as the ones we have discussed, are necessary (in addition to the basic cross section) in order to relate the scattering intensity over any specified bandwidth to the concentration of a particular constituent. Otherwise, significant errors in concentration analyses may be made, particularly in view of the fact that the total Q-branch scattering increases with vibrational excitation because of the factor $v+1$ in the upper-state band scattering.

M. Lapp
L. M. Goldman
C. M. Penney

General Electric Company
Corporate Research and Development, Schenectady, New York 12301

References and Notes

1. In other literature on Raman scattering and in infrared work these bands are often called hot bands, in reference to their appearance under thermally excited conditions. However, this phrase can be misleading, since upper-state bands can appear at low temperatures for species with low-lying vibrational energy levels. For example, Holzer *et al.* (*2*) have shown the importance of upper-state bands in Br_2 at room temperature. We have adopted the phrase "upper-state band" from R. M. Goody [*Atmospheric Radiation*, vol. 1, *Theoretical Basis* (Oxford Univ. Press, London, 1964), p. 21]. One further point of possible confusion lies in the conventional usage of vibrational "line" for the ground-state fundamental band. This terminology refers to the usually narrow Q-branches observed at room temperature, and so is not used here.
2. W. Holzer, W. F. Murphy, H. J. Bernstein, *J. Chem. Phys.* **52**, 399 (1970).
3. See, for a review, L. R. Bratzie and G. A. Oyen, *Spex Speaker* **14**, No. 1 (Dec. 1969) (published by Spex Industries, Inc., Metuchen, N.J.).
4. T. J. Barrett and A. Weber, *J. Opt. Soc. Amer.* **60**, 70 (1970); L. Y. Nelson, A. W. Saunders, Jr., A. B. Harvey, G. O. Neeley, *J. Chem. Phys.*, in press.
5. See, for example, W. E. Kaskan, in *Sixth Symposium (International) on Combustion* (Reinhold, New York, 1957), pp. 134–143.
6. G. F. Widhopf and S. Lederman, *Amer. Inst. Aeronaut. Astronaut. J.* **9**, 369 (1971).
7. The essential results appear for the case of a diatomic molecule and are in good agreement with experimental results. Calculations for polyatomic molecules are extremely more complicated.
8. G. Herzberg, *Molecular Spectra and Molecular Structure*, vol. 1, *Spectra of Diatomic Molecules* (Van Nostrand, Princeton, N.J., ed. 2, 1950), chap. 3. The spectroscopic constants subsequently used for N_2 and O_2 were taken from table 39.
9. ———, *Ibid.*, chap. 3, sections 2(e) and 2(f). L. A. Woodward, in *Raman Spectroscopy*, H. A. Szymanski, Ed. (Plenum, New York, 1967), p. 35.
10. J. B. Tatum, *Astrophys. J. Suppl. Ser.* **14** (No. 124), 21 (1967).
11. In this development, the wave number σ_0 is a function of both J and v. In Figs. 2, 3, and 4, the wavelength λ_0 is not simply the reciprocal of σ_0 but is defined as the wavelength corresponding to $J=0$ for the ground-state vibrational band.
12. The rotational partition function given here is evaluated for a $^2\Sigma$ state of a homonuclear molecule, which is the ground state for both N_2 and O_2. It includes the effect of nuclear spin [*ref.* 8].
13. See, for example, S. S. Penner, *Quantitative Molecular Spectroscopy and Gas Emissivities* (Addison-Wesley, Reading, Mass., 1959), chap. 17; J. Ashkenas and R. C. M. Learner, *Proc. Roy. Soc. Ser. A Math. Phys. Sci.* **301**, 355 (1967), and references cited therein.
14. R. Gaufres and S. Sportouch, *C. R. Hebd. Seances Acad. Sci. Paris* **272**, 995 (1971).
15. The calculated relative intensity data in Figs. 3 and 4 were obtained from the convolution of $S(v,J)$ values from Eq. 3 with the experimentally determined monochromator slit function, which indicates the relative response of the monochromator to the wave number σ when it is set at σ_0. These calculations were carried out through use of a computer. The slit function was found to be closely approximated by an isosceles triangle with only a very slight truncation. It is shown in Figs. 2A, 3A, and 4A normalized to the peaks of the ground-state bands. The spectral slit width Δ is the full width at half maximum. The inclusion of σ in Eq. 3 is not really necessary here because Δ is sufficiently large to always include many rotational lines simultaneously. For example, 16 N_2 rotational lines are within the spectral range 2Δ (the base of the slit function profile) of the low-wavelength edge of the ground-state band. We have neglected the O-branch ($\Delta J=-2$) Raman lines from this work although they are in the spectral range of interest, since they do not contribute any significant intensity for the cases investigated here. Their inclusion would, however, make the intensities of high upper-state bands less certain.
16. G. Herzberg, *Molecular Spectra and Molecular Structure*, vol. 2, *Infrared and Raman Spectra of Polyatomic Molecules* (Van Nostrand, Princeton, N.J., 1945), chap. 2, section 4, and chap. IV, section 4.
17. ———, *Ibid.*, p. 285.
18. We are grateful to G. E. Moore for his help in the combustion aspects of these experiments.

17 September 1971; revised 3 November 1971

U. S. GOVERNMENT AGENCIES

Central Intelligence Agency
Washington, D. C. 20505
ATTN: CRS/ADD/Publications

Institute for Defense Analyses
400 Army-Navy Drive
Arlington, Virginia 22202
ATTN: Dr. Hans G. Wolfhard,
Sen. Staff

Defense Documentation Center
Cameron Station
Alexandria, Virginia 22314

EPA Technical Center
Research Triangle Park
North Carolina 27711
ATTN: Dr. F. Herget, P-222

Arnold Air Force Station
Tennessee
ATTN: AEDC (DYF)

Arnold Air Force Station
Tennessee
ATTN: W. E. Smith Jr., Chief
T-Cells Division
Engine Test Facility

Air Force Eastern Test Range
MU-135
Patrick Air Force Base
Florida 32925
ATTN: AFETR Technical Library

Air Force Office of Scientific Research
1400 Wilson Boulevard
Arlington, Virginia 22209
ATTN: Dr. Joseph F. Masi

Air Force Aero Propulsion Laboratory
Wright-Patterson AFB, Ohio 45433
ATTN: [illegible]
Dr. Kenrya Mach

Air Force Aero Propulsion Laboratory
Wright-Patterson AFB, Ohio 45433
ATTN: Francis R. Ostdiek

Air Force Rocket Propulsion Laboratory
Department of Defense
Edwards AFB, California 93523
ATTN: LKCG (Mr. Selph)

U. S. Army Air Mobility Research and
Development Laboratory
Eustis Directorate
Fort Eustis, Virginia 23604
ATTN: Propulsion Division
(SAVDL-EU-PP)

U. S. Army Artillery Combat
Developments Agency
Fort Sill, Oklahoma
ATTN: Commanding Officer

U. S. Army Missile Command
Redstone Arsenal, Alabama 35809
ATTN: AMSMI-RR

U. S. Army Missile Command
Redstone Scientific Information Center
Redstone Arsenal, Alabama 35809
ATTN: Chief, Document Section

NASA
Deputy Director, Aeronautical Propulsion
Division, Code RC
Office of Advanced Research & Technology
Washington, D. C. 20546
ATTN: Mr. Nelson F. Rekos

NASA Ames Research Center
Deputy Chief Aeronautics Division
Mail Stop 27-0
Moffett Field, California 94035
ATTN: Mr. Edward W. Perkins

NASA Langley Research Center
Hampton, Virginia 23365
ATTN: Dr. Robert S. Levine
Mail Stop 213

NASA Lewis Research Center
21000 Brookpark Road
Cleveland, Ohio 44135
ATTN: D. Morris
Mail Stop 60-3

NASA Lewis Research Center
Hypersonic Propulsion Section
Mail Stop 6-1
21000 Brookpark Road
Cleveland, Ohio 44135
ATTN: Dr. Louis A. Povinelli

NASA Marshall Space Flight Center
SAE-ASTR-P
Huntsville, Alabama 35812
ATTN: Mr. Keith Chandler

National Science Foundation
Engineering Energetics
Engineering Division
Washington, D. C. 20550
ATTN: Dr. George Lee

National Science Foundation
Engineering Energetics
Engineering Division
Washington, D. C. 20550
ATTN: Dr. M. Gjelsa

National Science Foundation
Engineering Energetics
Engineering Division
Washington, D. C. 20550
ATTN: Dr. Royal Rosenbach

National Technical Information Service
Department of Commerce
5285 Port Royal Road
Springfield, Virginia 22151
ATTN: Chief, Input Section

U. S. Naval Air Development Center
Commanding Officer (AD-5)
Johnsville, Pennsylvania
ATTN: NADC Library

Naval Air Propulsion Test Center (PAT)
Trenton, New Jersey 08628
ATTN: Mr. Al Martino

Naval Air Systems Command
Department of the Navy
Washington, D. C. 20360
ATTN: Research Administrator
AIR 310

Naval Air Systems Command
Department of the Navy
Washington, D. C. 20360
ATTN: Propulsion Technology Adv.
AIR 330

Naval Air Systems Command
Department of the Navy
Washington, D. C. 20360
ATTN: Technical Library Division
AIR 604

U. S. Naval Ordnance Laboratory Commander
White Oak
Silver Springs, Maryland 20910
ATTN: Library

Naval Ordnance Systems Command
Department of the Navy
Washington, D. C. 20360
ATTN: ORD 0331

Naval Postgraduate School
Department of Aeronautics, Code 57
Monterey, California 93940
ATTN: Dr. Allen E. Fuhs

Naval Postgraduate School Superintendent
Monterey, California 93940
ATTN: Library (Code 2124)

U. S. Naval Postgraduate School
Monterey, California 93940
ATTN: Library, Code 2212

Office of Naval Research Branch Office
1030 East Green Street
Pasadena, California 91106
ATTN: Dr. Rudolph J. Marcus

Office of Naval Research
San Francisco Area Office
50 Fell Street
San Francisco, California 94102

Office of Naval Research Branch Office
536 S. Clark Street
Chicago, Illinois 60605
ATTN: Director

Office of Naval Research
New York Area Office
207 W. 24th Street
New York, New York 10011

Office of Naval Research Branch Office
495 Summer Street
Boston, Massachusetts 02210
ATTN: Director

Office of Naval Research
Power Branch, Code 473
Department of the Navy
Arlington, Virginia 22217

Office of Naval Research
Fluid Dynamics Branch
Code 438
Department of the Navy
Washington, D. C.
ATTN: Mr. Morton Cooper

Naval Research Lab
Code 7710
Washington, D. C. 20390
ATTN: M. W. Schauz

U. S. Naval Research Laboratory Director
Washington, D. C. 20390
ATTN: Technical Information Div.

Naval Research Laboratory Director
Washington, D. C. 20390
ATTN: Library Code 2629 (ONRL)

Naval Ship Research and Development Ctr.
Annapolis Division
Annapolis, Maryland 21402
ATTN: Library, Code A214

Naval Ship Systems Command
Department of the Navy
Washington, D. C. 20360
ATTN: Technical Library

Naval Weapons Center Commander
China Lake, California 93555
ATTN: Airbreathing Propulsion
Branch Code 4583

Naval Weapons Center
Chemistry Division
China Lake, California 93555
ATTN: Dr. William S. McEwan
Code C05

U. S. Naval Weapons Center
Commander
China Lake, California 93555
ATTN: Technical Library

U. S. Naval Weapons Center
Code 608
Thermochemistry Group
China Lake, California 93556
ATTN: Mr. Edward W. Price, Head

U. S. Naval Weapons Laboratory
Dahlgren, Virginia 22448
ATTN: Technical Library

Navy Underwater Systems Center
Fort Trumbull
New London, Connecticut 06320
ATTN: Technical Library

Picatinny Arsenal
Commanding Officer
Dover, New Jersey 07801
ATTN: Technical Information Library

State Documents Section
Exchange and Gift Division
Washington, D. C. 20540
ATTN: Library of Congress

LABORATORIES AND COMPANIES

AeroChem Research Laboratories, Inc.
P. O. Box 12
Princeton, New Jersey 08540
ATTN: Dr. Arthur Fontijn

AeroChem Research Laboratories, Inc.
P. O. Box 12
Princeton, New Jersey 08540
ATTN: Library

Aerojet Liquid Rocket Company
P. O. Box 13222
Sacramento, California 95813
ATTN: Technical Information Center

Aeronautical Res. Assoc. of Princeton
50 Washington Road
Princeton, New Jersey 08540
ATTN: Dr. Guido Sandri

Aerospace Corporation
Propulsion Department
1111 East Mill Street
San Bernardino, California
ATTN: Mr. Alexander Murazzow

Aeroprojects, Inc.
West Chester
Pennsylvania 19380

Atlantic Research Corporation
Shirley Highway and Edsall Road
Alexandria, Virginia 22314
ATTN: Librarian

Atlantic Research Corporation
Shirley Highway at Edsall Road
Alexandria, Virginia 22314
ATTN: Dr. Andrej Macek

Atlantic Research Corporation
Shirley Highway at Edsall Road
Alexandria, Virginia 22314
ATTN: Dr. Kermit E. Woodcock
Manager, Propulsion

AVCO Everett Research Laboratory
2385 Revere Beach Parkway
Everett, Massachusetts 02149
ATTN: Mr. Donald Leonard

AVCO Everett Research Laboratory
Everett, Massachusetts 02149
ATTN: Librarian

AVCO Lycoming Corporation
550 South Main Street
Stratford, Connecticut 06497
ATTN: Mr. John M. Schrader
Asst. Director R & D

Ballistics Research Laboratory
Commanding Officer
Aberdeen Proving Ground, Maryland
ATTN: Library

Battelle
Columbus Laboratories
505 King Avenue
Columbus, Ohio 43201
ATTN: Mr. Robert A. Putnam
Atmospheric Chemistry and
Combustion Systems Dir.

Beech Aircraft Corporation
9709 East Central
Wichita, Kansas 67206
ATTN: William R. Byrne, Jr.

Bell Aerospace Company
P. O. Box 1
Buffalo, New York 14240
ATTN: Dr. John H. Morgenthaler
C-81

Bell Aerospace Company
Advanced Technology Research
P. O. Box 1
Buffalo, New York 14240
ATTN: Dr. George Rudinger C-86

Bell Aerospace Company
P. O. Box 1
Buffalo, New York 14240
ATTN: Technical Library

Bureau of Mines
Bartlesville Energy Research Center
Box 1398
Bartlesville, Oklahoma 74003

Convair Aerospace Division
Manager of Propulsion
P. O. Box 748
Fort Worth, Texas 76101
ATTN: L. H. Schreiber

Cornell Aeronautical Laboratory, Inc
Aerodynamic Research Department
P. O. Box 235
Buffalo, New York 14221
ATTN: Dr. John W. Daiber

Esso Research and Engineering Company
Government Research Laboratory
P. O. Box 8
Linden, New Jersey 07036
ATTN: Dr. William F. Taylor
Senior Research Engineer

Fairchild Industries
Fairchild Republic Division
Farmingdale, New York 11735
ATTN: Engineering Library

Flame Research, Inc.
P. O. Box 10502
Pittsburgh, Pennsylvania 15235
ATTN: Dr. John Kenton

Forest Fire and Engineering Research
Pacific Southwest Forest & Range
Experiment Station
P. O. Box 245
Berkeley, California 94701
ATTN: Assistant Director

Garrett Corporation
AiResearch Manufacturing Company
Sky Harbor Airport
402 South 36th Street
Phoenix, Arizona 85034
ATTN: Mr. Alan L. Bennett, Manager
Aircraft Propulsion Engine
Product Line

General Dynamics
Electro Dynamic Division
P. O. Box 2507
Pomona, California 91766
ATTN: Library 52 6-20

General Dynamics
P. O. Box 748
Fort Worth, Texas 76101
ATTN: Technical Library
Mail Zone 2246

General Electric Company
AEG Technical Information Center
Mail Drop 1-32, Building 700
Cincinnati, Ohio 45215
ATTN: J. J. Brady

General Electric Space Sciences Lab
Valley Forge Space Tech. Center
Room M-5144
P. O. Box 8555
Philadelphia, Pennsylvania 19101
ATTN: Dr. Theodore Bauer

General Motors Corporation
Detroit Diesel-Allison Division
P. O. Box 894
Indianapolis, Indiana 46206
ATTN: Mr. Willard E. Barrett, Chief
Engineer, Advanced Development
Mail Drop U-27

General Motors Technical Center
Director, Passenger Car Turbine Dev.
General Motors Engineering Staff
Warren, Michigan 48090
ATTN: D. F. Hagey

Grumman Aerospace Corporation
Manager Space Vehicle Development
Bethpage, New York
ATTN: Mr. O. S. Williams

Mr. Daniel L. Hardison
11131 Embassy Drive
Cincinnati, Ohio 45240

Hercules Incorporated
Allegany Ballistics Laboratory
P. O. Box 210
Cumberland, Maryland 21502
ATTN: Mrs. Louise S. Derrick
Librarian

Hercules Incorporated
P. O. Box 98
Magna, Utah 84044
ATTN: Library 100-A

A/S Kongsberg Vaapenfabrikk
Gas Turbine Division
3601 Kongsberg, Norway
ATTN: R. E. Stanley
Senior Aerodynamicist

LTV Vought Aeronautics Company
Flight Technology, Project Engineer
P. O. Box 5907
Dallas, Texas 75222
ATTN: Mr. James C. Otterbach

Lockheed-Georgia Company
Dept. 72-47, Zone 259
Marietta, Georgia 30060
ATTN: William A. French

Lockheed Missiles & Space Company
3251 Hanover Street
Palo Alto, California 94304
ATTN: Palo Alto Library 52-52

Lockheed Propulsion Company
Scientific and Technical Library
P. O. Box 111
Redlands, California 92373
ATTN: Head Librarian

Los Alamos Scientific Laboratory
P. O. Box 1663
Los Alamos, New Mexico 87544
ATTN: J. Arthur Freed

The Marquardt Company
501 Aerospace Corporation
16555 Saticoy Street
Van Nuys, California 91409
ATTN: Library

Martin-Marietta Corporation
P. O. Box 179
Denver, Colorado 80201
ATTN: Research Library 6617

Martin-Marietta Corporation
Orlando Division
P. O. Box 5837
Orlando, Florida 32805
ATTN: Engineering Library, mp-30

McDonnell Aircraft Company
P. O. Box 516
St. Louis, Missouri 63166
ATTN: Research & Engineering Library
Dept. 218 - Bldg. 103

McDonnell Douglas Corporation
Project Propulsion Engineer
Dept. 283, Bldg. 65, Level 2S
P. O. Box 516
St. Louis, Missouri 63166
ATTN: Mr. William C. Patterson

McDonnell Douglas Corporation
Research Laboratories
St. Louis, Missouri 63166
ATTN: Niklas Sojbeh
Associate Scientist

McDonnell Douglas Astronautics Company
5301 Bolsa Avenue
Huntington Beach, California 92647
ATTN: A3-329 Technical Library
Services

National Research Council
Division of Mechanical Engineering
Montreal Road, Ottawa
Ontario, Canada K1A 0R6
ATTN: Dr. R. B. Whyte

Nielsen Engineering & Research, Inc.
850 Maude Avenue
Mountain View, California 94040
ATTN: Dr. Jack N. Nielsen

Nissan Motor Company, Ltd.
3-5-1, Moto-, Sugimachi-ku
Tokyo, Japan 167
ATTN: Dr. Y. Toda

Northrop Corporation
Ventura Division
1515 Rancho Conejo Boulevard
Newbury Park, California
ATTN: Technical Interest

Norwegian Defense Research Establishment
Superintendent NDRE
P. O. Box 25
2007 Kjeller, Norway
ATTN: Mr. T. Krog

ONERA
Energie and Propulsion
29 Avenue de la Division Leclerc
92 Chatillon sous Bagneux, France
ATTN: Mr. M. Barrere

ONERA
Energie and Propulsion
29 Avenue de la Division Leclerc
92 Chatillon sous Bagneux, France
ATTN: Mr. J. Fabri

ONERA
Energie and Propulsion
29 Avenue de la Division Leclerc
92 Chatillon sous Bagneux, France
ATTN: Mr. Viaud

Professor S. Pessiliton
Residence les Closeaux, #22
109, Route de Morsang
91, Saintry, France

Mr. J. Richard Perrin
16261 Garcia Avenue
Encino, California 91316

Philco-Ford Corporation
Aeronautic Division
Ford Road
Newport Beach, California 92663
ATTN: Technical Information Service

Pratt and Whitney Aircraft
Project Engineer, Advanced Military
Engineering Dept. - 2B
East Hartford, Connecticut 06108
ATTN: Mr. Donald S. Rudolph

Pratt and Whitney Aircraft Division
United Aircraft Company
400 S. Main Street
East Hartford, Connecticut 06108
ATTN: Mr. Dana E. Waring
Manager-Product Technology

Pratt and Whitney Aircraft
Program Manager, Advanced Military Eng.
Engineering Department - 2B
East Hartford, Connecticut 06108
ATTN: Dr. Robert T. Stroup

Pratt and Whitney Aircraft
Florida Research and Development Ctr.
P. O. Box 2691
West Palm Beach, Florida 33402
ATTN: Dr. Richard B. Schweiger - 860
Senior Program Manager

RCA Corporation
Missile and Surface Radar Division
Moorestown, New Jersey 08057
ATTN: Engineering Library
Bldg. 101-222

Rocket Research Corporation
11441 Willow Road
Redmond, Washington 98052
ATTN: Thomas A. Groudle

Rocketdyne Division
North American Rockwell
6633 Canoga Avenue
Canoga Park, California 91304
ATTN: Technical Information Center
D/596-108

Rocketdyne Division
North American Rockwell
6633 Canoga Avenue AA67
Canoga Park, California 91304
ATTN: Mr. Henry C. Wiesneck
Manager

Rohr Corporation
Manager Advanced Technology
Engineering Division
Chula Vista, California 92012
ATTN: Mr. Joseph S. Mount

Sandia Laboratories
P. O. Box 969
Livermore, California
ATTN: Dr. Dan Hartley, Div. 8351

Sandia Laboratories
P. O. Box 5800
Albuquerque, New Mexico 87115
ATTN: Technical Library, 3141

Solar
2200 Pacific Highway
San Diego, California 92112
ATTN: Librarian

Standard Oil Company (Indiana)
P. O. Box 400
Naperville, Illinois 60540
ATTN: R. E. Pritz

Teledyne CAE
1330 Laskey Road
Toledo, Ohio 43601
ATTN: Technical Library

TRW Systems
One Space Park
Bldg. 01 Room 2260
Redondo Beach, California
ATTN: Mr. Donald M. Lee, Manager

TRW Systems
One Space Park
Redondo Beach, California 90278
ATTN: Mr. F. E. Fendell (R1/1004)

United Aircraft Research Laboratory
400 Main Street
East Hartford, Connecticut 06108
ATTN: Dr. Frank Carta

United Aircraft Research Laboratory
400 Mai Street
East Hartford, Connecticut 06108
ATTN: Librarian

Valley Forge Space Tech. Center
P. O. Box 8555
Philadelphia, Pennsylvania 19101
ATTN: Dr. Beryl Zaidmer

Vought Missiles & Space Company
P. O. Box 6267
Dallas, Texas 75222
ATTN: Library - 3-81000

Polytechnic Institute of Brooklyn
Department of Aerospace Engineering
and Applied Mechanics
Brooklyn, New York
ATTN: Dr. Samuel Lederman

Brown University
Division of Engineering
Box D
Providence, Rhode Island 02912
ATTN: Dr. R. A. Dobbins

California Institute of Technology
Department of Chemical Engineering
Pasadena, California 91109
ATTN: Prof. W. H. Corcoran

California Institute of Technology
Jet Propulsion Laboratory
4800 Oak Grove Drive
Pasadena, California 91103
ATTN: Library

University of California, San Diego
Dept. of Aerospace and Mechanical
Engineering
La Jolla, California
ATTN: Professor Paul Libby

University of California, San Diego
Dept. Of Engineering Physics
P. O. Box 109
La Jolla, California 92037
ATTN: Professor S. S. Penner

University of California
School of Engineering and
Applied Science
7513 Boelter Hall
Los Angeles, California 90024
ATTN: Engineering Reports Group

University of California
Lawrence Radiation Laboratory
P. O. Box 808
Livermore, California 94550
ATTN: Technical Information Dept.
L-3

University of California
General Library
Berkeley, California 94720
ATTN: Documents Department

Case Western Reserve University
10900 Euclid Avenue
Cleveland, Ohio 44106
ATTN: Sears Library - Reports Dept.

Case Western Reserve University
Division of Fluid Thermal and
Aerospace Sciences
Cleveland, Ohio 44106
ATTN: Professor Eli Reshotko

Colorado State University
Engineering Research Center
Fort Collins, Colorado 80521
ATTN: Mr. V. A. Sandborn

The University of Connecticut
Department of Aerospace Engineering
Storrs, Connecticut 06268
ATTN: Dr. P. Frank Hochett
Associate Professor

Cooper Union
School of Engineering and Science
Cooper Square
New York, New York
ATTN: Dr. Wallace Chintz
Associate Professor of ME

Cornell Aeronautical Laboratory, Inc.
4455 Genessee Street
Buffalo, New York 14221
ATTN: Head Librarian

Cornell University
Department of Chemistry
Ithaca, New York 14850
ATTN: Prof. Simon H. Bauer

Technical University of Denmark
Fluid Mechanics Department
Building 404 2800 Lyngby
DK-Denmark
ATTN: Professor K. Refslund

Franklin Institute Research Laboratories
Philadelphia, Pennsylvania 19103
ATTN: Dr. G. P. Wachtell

Fysisch Laboratorium
Rijksuniversiteit Utrecht
Sorbonnelaan
Utrecht, The Netherlands
ATTN: Dr. F. van der Walt

Georgia Institute of Technology
Atlanta, Georgia 30332
ATTN: Price Gilbert Memorial Library

Georgia Institute of Technology
School of Aerospace Engineering
Atlanta, Georgia 30332
ATTN: Dr. Ben T. Zinn
Professor

University of Illinois
Department of Energy Engineering
Box 4348
Chicago, Illinois 60680
ATTN: Professor Paul N. Chang

University of Illinois
College of Engineering
Dept. of Energy Engineering
Chicago, Illinois
ATTN: Dr. D. S. Hacker

Imperial College
London, England
ATTN: Professor Gaydon

Imperial College of Science & Technology
Department of Mechanical Engineering
Exhibition Road
London, S.W.7, England
ATTN: Professor W. Margetroyd

The Johns Hopkins University
Applied Physics Laboratory
8621 Georgia Avenue
Silver Spring, Maryland 20910
ATTN: Chemical Propulsion
Information Agency

The Johns Hopkins University
Applied Physics Laboratory
8621 Georgia Avenue
Silver Spring, Maryland 20910
ATTN: Document Librarian

The Johns Hopkins University
Applied Physics Laboratory
8621 Georgia Avenue
Silver Spring, Maryland 20910
ATTN: Dr. A. A. Westenberg

University of Leeds
Leeds, England
ATTN: Professor Dixon-Lewis

Massachusetts Institute of Technology
Dept. of Chemical Engineering
Cambridge, Massachusetts 02139
ATTN: Dr. Jack B. Howard

Massachusetts Institute of Technology
Department of Chemistry, Room 6-123
Cambridge, Massachusetts 02139
ATTN: Dr. John Ross

MIT Libraries Room 14 E-210
77 Massachusetts Avenue
Cambridge, Massachusetts 02139
ATTN: Technical Reports

Massachusetts Institute of Technology
Room 10 405
Cambridge, Massachusetts 02139
ATTN: Engineering Technical Reports

Massachusetts Institute of Technology
Dept. of Mechanical Engineering
Room 3-246
Cambridge, Massachusetts 02139
ATTN: Professor James Fay

Massachusetts Institute of Technology
Dept. of Mechanical Engineering
Cambridge, Massachusetts 02139
ATTN: Prof. Robert E. Stickney

University of Michigan
Department of Aerospace Engineering
Ann Arbor, Michigan 48105
ATTN: Prof. T. C. Adamson, Jr.

Midwest Research Institute
425 Volker Boulevard
Kansas City, Missouri 64100
ATTN: Dr. T. A. Milne

Mitglied des Vorstands der Fried.
Krupp GmbH
43 Essen, Altendorferstraße 103
Germany
ATTN: Professor Dr.-Ing.
Wilhelm Oetbering

New York Institute of Technology
Wheatley Road
Old Westbury, New York 11568
ATTN: Dr. Fox

University of Notre Dame
College of Engineering
Notre Dame, Indiana 46556
ATTN: Stuart T. McComas, Asst. Dean
for Research & Special Projects

Ohio State University
Dept. of Chemical Engineering
140 West 19th Avenue
Columbus, Ohio
ATTN: Dr. Robert S. Brodkey

The Pennsylvania State University
Room 207 Old Main Building
University Park, Pennsylvania 16802
ATTN: Office of Vice President
for Research

Pennsylvania State University
College of Engineering
University Park, Pennsylvania 16802
ATTN: Dr. Otis E. Lancaster
Prof. of Engineering Education

Institute Politechnico Nacional
Unidad Profesional de Zacatenco
Mexico 14, D. F. Mexico
ATTN: Ing. Manuel Zorrilla
Director General

Princeton University
Dept. of Aerospace and Mech. Sciences
James Forrestal Campus
Princeton, New Jersey 08540
ATTN: Dr. Martin Summerfield

Princeton University
Forrestal Campus Library
P. O. Box 710
Princeton, New Jersey 08540
ATTN: V. A. Simosko, Librarian

Purdue University
School of Mechanical Engineering
Lafayette, Indiana 47907
ATTN: Prof. V. W. Goldschmidt

Purdue University
School of Mechanical Engineering
Lafayette, Indiana 47907
ATTN: Professor S. L. K. Wittig

Purdue University
School of Aeronautics, Astronautics,
and Engineering Sciences
Lafayette, Indiana 47907
ATTN: Library

Queen Mary College
Dept. of Mechanical Engineering
Thile Eld Road
London El, England
ATTN: Professor M. W. Thring

Rice University
Welch Professor of Chemistry
Houston, Texas 77001
ATTN: Dr. Joseph L. Franklin

University of Rochester
Department of Chemical Engineering
Rochester, New York 14627
ATTN: Dr. John R. Ferron

Rome University
Via Bradano 28
00153 Rome, Italy
ATTN: Prof. Gaetano Salvatore

Sophia University
Science and Engineering Faculty
Kioi 7 Tokyo-Chiyoda Japan 102
ATTN: Professor M. Suzuki

Stanford Research Institute
Dept. of Chemical Dynamics
Menlo Park, California 94025
ATTN: Dr. Henry Wise

Stanford University
Dept. of Aeronautics and Astronautics
Stanford, California 94305
ATTN: Dr. Walter G. Vincenti

Stanford University
Dept. of Mechanical Engineering
Stanford, California 94305
ATTN: Professor A. L. London

Stevens Research Institute
Castle Point Station
Hoboken, New Jersey 07030
ATTN: Prof. Robert F. McAlevy III
Combustion Lab Director

University of Tokyo
Dept. of Reaction Chemistry
Faculty of Engineering
Bunkyo-ku
Tokyo, Japan 113
ATTN: Professor T. Hikita

University of Virginia
Dept. of Aerospace Engineering
School of Engr. and Applied Science
Charlottesville, Virginia 22901
ATTN: Dr. John E. Scott

University of Virginia
Science/Technology Information Center
Charlottesville, Virginia 22901
ATTN: Richard K. Austin

Virginia Polytechnic Institute and
State University
Dept. of Aerospace Engineering
Blacksburg, Virginia 24061
ATTN: Dr. George R. Inger

Virginia Polytechnic Institute and
State University
Mechanical Engineering Dept.
Blacksburg, Virginia 24061
ATTN: Mr. Walter S. O'Brien, Jr.

The George Washington University
Washington, D. C. 20006
ATTN: Reports Section

Yale University
Engineering and Applied Science
Mason Laboratory
New Haven, Connecticut 06520
ATTN: Dr. John B. Fenn

Yale University
Mason Laboratory
400 Temple Street
New Haven, Connecticut 06520
ATTN: Prof. Peter P. Wegener